Al-Darraji, F, Sadique, MM, Alahmari, TS, Yu, Z, Shubbar, A and Marolt Cebasek, T

Investigation of new confined concrete-filled aluminum tube piles: Experimental and numerical approaches

Article

Journal Pre-proof

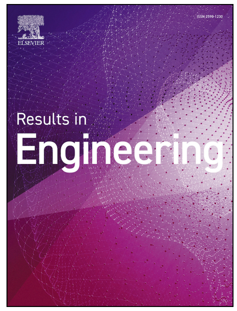

Investigation of new confined concrete-filled aluminum tube piles: Experimental and numerical approaches

Fadhil Al-Darraji, Monower Sadique, Turki S. Alahmari, Zelong Yu, Ali Shubbar, Tina Marolt Cebasek

PII: S2590-1230(24)01379-3

DOI: https://doi.org/10.1016/j.rineng.2024.103124

Reference: RINENG 103124

To appear in: *Results in Engineering*

Received Date: 26 July 2024

Revised Date: 5 October 2024

Accepted Date: 12 October 2024

Please cite this article as: F. Al-Darraji, M. Sadique, T.S Alahmari, Z. Yu, A. Shubbar, T. Marolt Cebasek, Investigation of new confined concrete-filled aluminum tube piles: Experimental and numerical approaches, *Results in Engineering*, https://doi.org/10.1016/j.rineng.2024.103124.

Investigation of new confined concrete-filled aluminum tube piles: Experimental and numerical approaches

Fadhil Al-Darraji[1,2,*], Monower Sadique[2], Turki S. Alahmari[3], Zelong Yu[2], Ali Shubbar[2] ,Tina Marolt Čebašek[2]

[1]Department of Civil Engineering, College of Engineering, University of Basrah, Basrah, Iraq
[2]School of Civil Engineering and Built Environment, Liverpool John Moores University,
Liverpool L3 3AF, UK; m.m.sadique@ljmu.ac.uk (M.S.); z.yu@ljmu.ac.uk (Z.Y.); A.A.Shubbar@ljmu.ac.uk and t.maroltcebasek@ljmu.ac.uk (T.M.Č.).
[3] Department of Civil Engineering, Faculty of Engineering, University of Tabuk, P.O. Box 741, Tabuk 71491, Saudi Arabia: talahmari@ut.edu.sa

[*]Corresponding author: f.k.aldarraji@2021.ljmu.ac.uk

Abstract

This research aims to introduce and test a Confined Concrete-Filled Aluminum Tube Pile (CCFAT) as an innovative composite pile that embodies a distinctive amalgamation of favourable material characteristics. Experimental tests were carried out to achieve this goal by analysing the vertical and lateral responses of various configurations and slenderness ratios (L_m/D) (ranging from 10 to 20) of CCFAT piles. As a reference group, two traditional piles were also manufactured and tested under identical conditions for comparison purposes. Additionally, the finite element approach was applied to validate the experimental results. The findings indicated that CCFAT piles have either higher or at least equivalent ultimate vertical capacity to that of reference piles. Additionally, the results proved the superior ultimate lateral capacity of the CCFAT piles compared to the reference ones. The results also showed a constant maximum bending moment dept in the CCFAT piles with a L_m/D ratio of 10, with a slight increase observed for CCFAT with a L_m/D ratio of 20 under lateral loading, which could be attributed to the rigidity of the CCAFT piles. Moreover, the outcomes of the finite element analysis indicated that both ultimate vertical and lateral capacities improve with the increase in the number of piles. The sensitivity analysis showed that the dilatancy angle plays the most important role in determining the vertical capacity of the piles, while the lateral capacity was significantly determined by the internal friction angle. Finally, fitted charts were produced and validated in this study to help researchers estimate the ultimate vertical and lateral capacities of CCFAT piles depending on the stiffness of the pile groups.

Keywords: Confined Concrete-Filled Aluminium Tube Pile, Composite pile, pile types, soil chamber, Pile group stiffness.

1. Introduction

Pile foundations are traditionally made from timber, steel, and concrete, offering versatility for different applications [1, 2]. Extensive research was conducted to understand the behaviour of piles in various subsurface conditions, installation methods, and also in marine environments that can give rise to various challenges[3-5]. The parameters studied included timber degradation, steel corrosion, and concrete deterioration caused by marine borer infestation [6]. Generally, the research outcomes showed that traditional materials employed for piling under such rigorous exposure conditions may result in limited operational lifespans and significant financial outlays for maintenance activities.

An emerging trend in deep foundations pertains to adopting composite piles, driven by their inherent merits surpassing traditional piles. The term "composite pile" predominantly denotes a structural arrangement comprising a composite tube that is infused with concrete material [7]. This tube functions as an integral structural casing, serving as both a mould for shaping the concrete and augmenting the overall rigidity of the system. Additionally, the composite tube provides a protective barrier against corrosion for the inner concrete core, consequently leading to a significant extension in the operational longevity of the pile units. Research about composite piles has predominantly centred on the individual response of piles when subjected to vertical and lateral loads. Various investigative approaches, encompassing laboratory experimentation, field observations, and numerical simulations, have been employed. Nevertheless, the investigation into the collective behaviour of piles within a group is notably limited, signifying a potentially innovative area for exploration. A review of some types of composite piles is presented in the following sections.

The prevalent composite pile system is typically characterised by the incorporation of concrete-filled Fibre-Reinforced Polymer (FRP) piles. Researchers have empirically illustrated that, when subjected to vertical loads, the FRP pile system outperforms comparable prestressed and reinforced concrete structural elements [8, 9]. Giraldo and Rayhani [10, 11] presented an experimental investigation on the performance of concrete-filled FRP piles and hollow FRP piles in clayey and soft clay. Small-scale FRP piles were manufactured and assessed to transfer loading. FRP material and fibre orientation have a significant influence on the vertical capacity, which was reported. At the same time, the lower stiffness of the FRP piles leads to increased pile head displacement under lateral loading compared to steel piles. Lu et al. [12] performed an experimental study to assess the factors that influence the behaviour of FRP piles under vertical and lateral loads in sandy soil. The FRP piles were tested in this experiment in a special pressure chamber. The results showed that the surface roughness, confining pressure, and relative density determined the shearing resistance of the soils and subsequently affected the bearing capacity of the FRP piles under a vertical load. Different types of FRP, pile size, and climate age all had an impact on the flexural stiffness of pile foundation.

Despite their commendable load-bearing characteristics, FRP composite piles exhibit certain potential limitations in terms of structural performance, primarily attributed to the relatively low stiffness of the constituent material in the pile tubes. Consequently, researchers endeavoured to enhance the fibre reinforcement by incorporating glass fibres, leading to the designation of these composite piles as Glass-Fibre-Reinforced Polymer piles (GFRP piles). To investigate the interface behaviour of GFRP piles in cohesionless soil, Almallah et al. [13] conducted a study involving the application of a silica sand coating on the surface of these piles. The research employed seven small-scale GFRP piles characterised by varying levels of surface roughness, with a reference steel pile serving as a control element. In this study, the surface of five out of the seven GFRP piles was coated with silica sand. The findings of the study revealed an innovative mechanism wherein the application of a silica sand coating on GFRP piles effectively increased the interface friction between the GFRP piles and the surrounding sand when subjected to axial loads. Consequently, this enhancement contributed to a notable increase in the ultimate load-bearing capacity of the piles, as compared to the control piles.

Nonetheless, the increased axial ultimate load-bearing capacity achieved through the reinforcement of the fibre and the application of a sand coating to the surface falls short of providing a comprehensive understanding of the response of heavier piles subjected to lateral loading. Furthermore, the limited stiffness inherent in the constituent material of the tube may continue to govern the lateral response of these piles. Therefore, a thorough investigation into the performance of composite piles under both axial and lateral loading conditions becomes imperative, potentially leading to the incorporation of a novel composite pile variant. Consequently, a dedicated study was conducted, wherein a composite pile composed of stainless steel and filled with standard mortar was fabricated, serving as the experimental specimen, while a hollow steel pile was employed as the reference. A series of experiments were undertaken involving both hollow piles and composite piles embedded within stratified soil, subjected to static axial, and static lateral loads. Various length-to-diameter ratios, specifically 10, 15, 20, 25, and 30, were considered by adjusting the pile length to emulate the behavior of stiff piles. The outcomes of the experimental investigations were subsequently validated through comparison with results obtained from finite element software ABAQUS. The collective findings derived from the experimental assessments and numerical analyses revealed that increasing the length-to-diameter ratios leads to an increase in load-carrying capacity and a concurrent reduction in settlement for both types of pile [14]. While Venkatesan et al. [14] may have successfully addressed the issue of low stiffness within the constituent material of FRP and GFRP, it is noteworthy that existing research has predominantly concentrated on elucidating the performance characteristics of individual composite piles. In practical applications, composite pile groups are more prevalent. Researchers reported that it is essential to recognise that the lateral behavior of pile groups becomes considerably more intricate due to the introduction of inter-pile interactions, which can significantly reduce the collective lateral bearing capacity [15-21].

A noticeable research gap persists regarding the behavioural analysis of composite pile groups subjected to both vertical and lateral loads. In order to address this gap of knowledge in the existing literature, the present study endeavours to comprehensively investigate the performance of composite piles, both in singular form and when organised into pile groups, under the influence of vertical and lateral loading. This investigation is conducted through the utilisation of scaled models and finite element simulations. The chosen configuration for the composite pile is a Confined Concrete-Filled Aluminium Tube Pile (CCFAT) pile, which embodies a distinctive amalgamation of the structural advantages offered by aluminium and concrete. CCFAT piles are typically fabricated by encapsulating an aluminium tube with concrete, thereby yielding a composite material characterised by its unique properties. The aluminium component equips the pile with an exceptional strength-to-weight ratio and corrosion resistance, while the concrete component contributes vital compressive strength and structural stiffness. Notwithstanding these notable attributes, it is worth noting that CCFAT piles constitute a relatively promising technology within the domain of geotechnical engineering, and the development of comprehensive design guidelines for their implementation remains an ongoing endeavour. Consequently, it becomes imperative to conduct further research endeavours to elucidate the optimal design and construction methodologies for CCFAT piles and gain a deeper understanding of their response to vertical and lateral loading conditions.

This research aims to gain insights into the performance of three different types of piles: Concrete-Filled Aluminium Tube (CCFAT) piles, Hollow Aluminium Tube (HAT) piles, and Precast Concrete (PC) piles. The study uses laboratory tests to compare the vertical and lateral performance of these pile types. Thereafter, the researchers conducted finite element (FE) analysis to further investigate the response of CCFAT pile foundations under vertical and lateral loading conditions. This involved validating the FE model and then using it to study larger pile groups. Based on the FE results, expressions have been proposed to determine the vertical and lateral stiffness of pile groups, taking into account the number of piles. The study also explores the load transfer mechanisms of the different pile configurations under vertical and lateral loads. Finally, sensitivity analyses have been performed to determine the influencing parameters on the vertical and lateral response of CCFAT pile group foundations.

2. Experimental setup and instrumentation

2.1. Pile models

Experimentally, 12 CCFAT piles and two traditional types of piles (reference groups), namely hollow aluminium tube (HAT) piles and precast concrete (PC) piles, were prepared for the experimental work. Table 1 lists the configurations of the piles, as shown in Figure 1. The CCFAT piles were fabricated using aluminium tubes (38.1 mm in diameter and wall thickness of 1.6 mm) filled with concrete (having a compressive strength of fc =30 MPa). The lengths of CCFAT piles were chosen to maintain slenderness ratios (embedment length-to-diameter) of 10, 15 and 20 [22]. The dimensions of the aluminium tube were selected based on commercially available measurements to meet the required slenderness ratios while minimizing boundary effects related to the rig dimensions. The concrete mix design was optimized to ensure adequate workability and compaction, aligning closely with the material properties recommended for both aluminium and concrete, as noted by [23]. Experimentally, single and two-group configurations i.e., 2x1 and 2x2 pile groups, were tested under vertical and lateral loading schemes.

Aluminium plates of 20 mm in thickness were used to fabricate pile caps according to the desired dimensions and then drilled to match the configuration of the pile. The distances, centre-to-centre, between piles in each group were three times the pile diameter (S = 3D). The dimensions of pile caps for models pile single, 1x2, and 2x2 were 100x100mm,200x100mm, and 200x200mm respectively. Figure 2 shows the CCFAT piel details and the pie caps dimensions. Other studies have indicated that the optimal center-to-center spacing between piles within a group is equivalent to three times the diameter of the pile [24-26].

It is noteworthy to highlight that HAT and PC piles were manufactured using the same aluminium tubes and concrete used to manufacture the CCFAT piles, respectively. The lengths of HAT and PC piles were chosen to maintain a L_m/D ratio of 10, and they were set up as a 2x1 pile group configuration, and the piles' caps had the exact dimensions and specifications of those used with the CCFAT piles.

Table 1. Configuration of pile models

Pile configuration	L_m/D	Pile diameter, D (mm)	Pile spacing S/D	Pile type
Single	10	38.1	-	CCFAT pile
	15	38.1	-	CCFAT pile
	20	38.1	-	CCFAT pile
2x1	10	38.1	3	CCFAT pile
	15	38.1	3	CCFAT pile
	20	38.1	3	CCFAT pile
	10	38.1	3	HAT pile
	10	38.1	3	PC pile
2x2	10	38.1	3	CCFAT pile
	15	38.1	3	CCFAT pile
	20	38.1	3	CCFAT pile

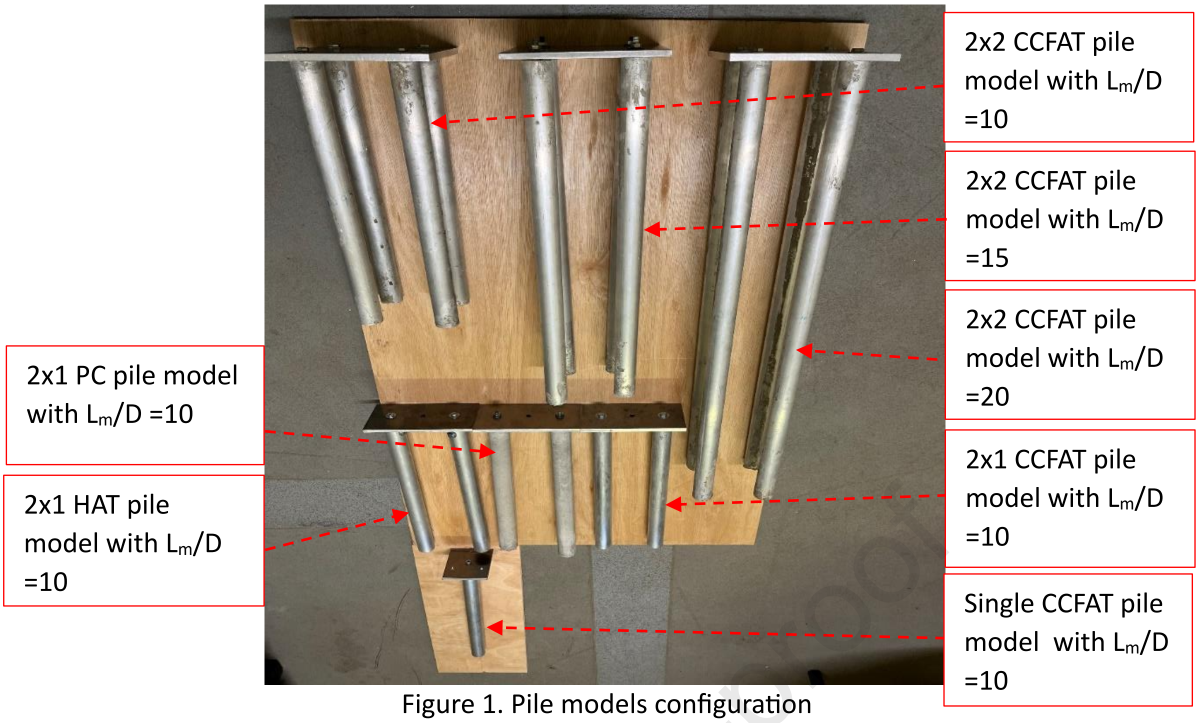

Figure 1. Pile models configuration

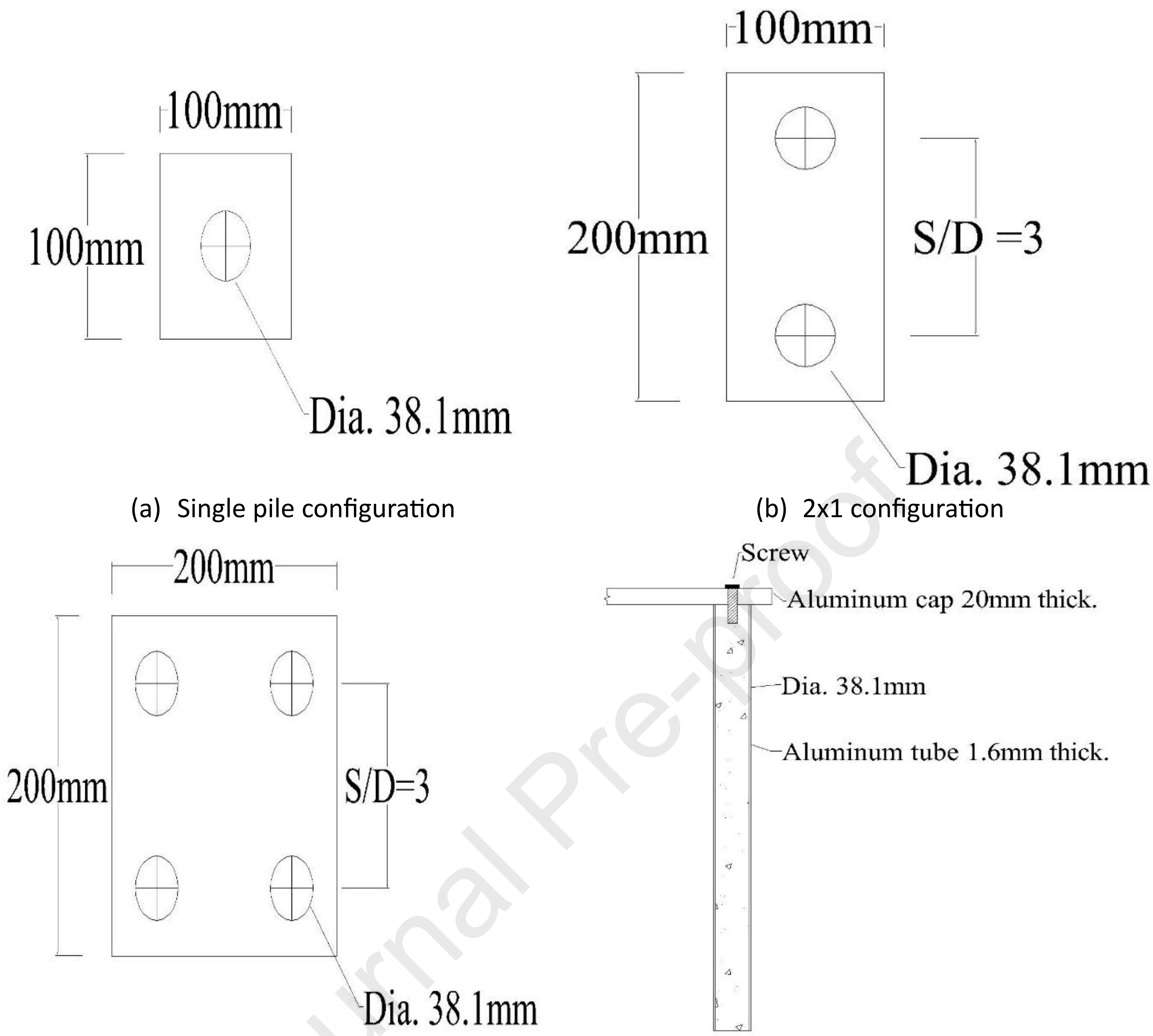

(a) Single pile configuration (b) 2x1 configuration

(c) 2x2 configuration (d) CCFAT pile model

Figure 2. Pile caps dimensions and CCFAT pile detail

2.2. Soil properties

In this study, fine-grained loose sand, obtained from a local supplier, was utilized as the primary material. Figure 3a illustrates the utilisation of scanning electron microscopy (SEM) at a 40x magnification with a working distance (WD) of 10.2 mm for the examination of the morphology of sand within the experimental framework. The observations revealed that the sand particles exhibited a sub-rounded morphology, which contributes to an elevated unit weight compared to fully rounded particles. Essential sand sample characteristics, such as classification, and specific gravity were determined in accordance with the guidelines outlined in BS EN 1377-2:2022 [27] Figure 3b graphically depicts the particle size distribution of the sand. According to the Unified Soil Classification System (USCS), the utilised sand material may be categorised as poorly graded (SP). The sample's Coefficient of Curvature (C_c) and Coefficient of Uniformity (C_u) were determined to be 1.11 and 1.9, respectively. The sand density was verified using the known weight and volume of a small mold. After vibrating the sand, its specific density was determined. The following equation was used to establish the sand test beds.

$$D_r = \frac{\gamma_{max}(\gamma_d - \gamma_{min})}{\gamma_d\,(\gamma_{max} - \gamma_{min})} \quad (1)$$

Here, D_r is the relative density of sand and γ_{max}, γ_{min}, and γ_d are the maximum, minimum, and dray density for sand (kN/m^3), respectively. the density of sand was used to analyze the influence of sand on the CCFAT piles model response. that density was 16.065 kN/m^3, which represents a relative density (D_r) of 30%. To address scale factor challenges and accurately replicate in-situ pile-load testing, it is essential to preserve the influence of grain size distribution on the combined pile-soil interaction. this research maintained a ratio of 112 between the diameter of the pile and the diameter of the sand medium (D/D_{50}). Recommendations by various researchers stipulate a minimum ratio of 60 for the pile diameter (D) to the medium diameter of the sand (D_{50}) [28]. However, Garnier et al [29] proposed a lower threshold value for the ratio at 100.

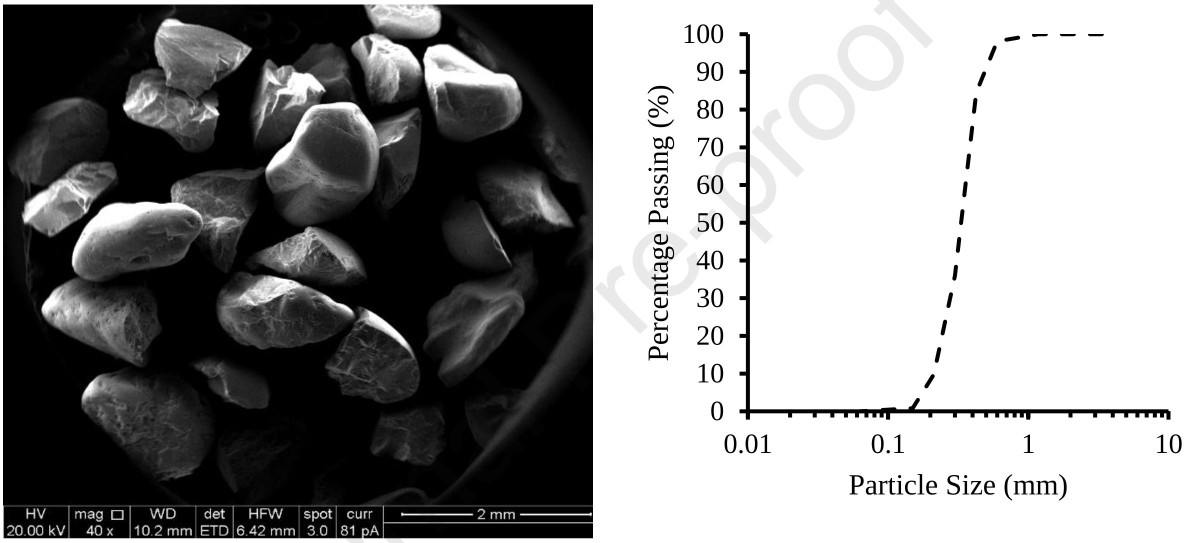

(a) SEM for sand sample, HV=20.00kV, mag=40x, WD= 10.2 mm

(b) Distribution of sand particles according to size

Figure 3. Sand properties

2.3. Soil preparation

The pouring and tamping technique was adapted in this stage of the study to lay sand in the test machine; the sand was layered, and each layer was tamped to achieve the desired relative density (D_r) of 30% [30-35]. Practically, the layering of the sand soil was carried out firstly by dividing the height of the chamber into 50 mm layers. Secondly, the sand with a previously estimated and weighed quantity was transferred to the testing chamber using a scoop. Thirdly, a hand compactor was used to compact each single layer to the desired depth. To achieve the desired result of relative density, the scoop was placed as close as possible to the surface of the previous sand layer. The surface of the granular soil layer was levelled horizontally using a water balance. The density of each sand layer was evaluated by positioning five containers. The results demonstrated that the variation in density was nearly insignificant.

2.4. Testing rig setup

The experimental apparatus comprises a square-sectioned enclosure soil chamber, which was designed and constructed at Liverpool John Moores University (LJMU). The dimensions of the chamber are 900 mm (W) x 900 mm (L) x 1250 mm (H). The experimental rig was configured to accommodate the application of both vertical and lateral loads to either individual or pile group models. To administer vertical loads to the singular pile or pile group models, a hydraulic ram was securely affixed to two structural beams within the soil chamber, with the hydraulic ram positioned atop a reaction beam measuring 150 mm x 75 mm x 18 mm (U-shaped profile). In addition to vertical loading capabilities, the testing rig was also equipped to apply lateral loads. For the purpose of lateral load tests, a dedicated horizontal reaction beam was custom-fabricated to furnish the requisite reaction force against the applied lateral loads acting upon the single pile or pile groups model. The lateral loads are also administered using a hydraulic ram identical to the one used for vertical loading.

2.5. Experimental setup

The schematic representation of the experimental arrangement employed for conducting vertical load tests on the pile models is depicted in Figure 4a. The vertical loading system encompasses a precisely calibrated load cell attached to the apex of the pile model cap, linked to an adjustable pin with a series of perforations along an extendable rod spanning up to 1.5 m. This rod was securely fastened to a vertical hydraulic arm, and the hydraulic pump is responsible for administering the vertical load. Two linearly variable differential transducers (LVDTs) were strategically positioned equidistant from the centre of the model to monitor the vertical displacement of the pile cap during loading. A 16-bit resolution data acquisition system was employed for recording both the vertical load and associated movement. It is noteworthy that the pile models underwent driving to specific depths, attaining staffed required (L_m/D) ratios of 10, 15, and 20, utilising the identical vertical hydraulic loading mechanism. The total pile length was defined as the sum of the embedment length and an additional freestanding length of 150 mm to prevent soil contact with the pile cap. This approach ensures that the bearing capacity of the pile, as determined through testing, is solely attributed to soil-pile interaction, eliminating any influence from direct load transfer to the soil surface.

In the lateral load system, the load cell, accompanied by the adjustable pile, was connected to a hydraulic arm oriented horizontally towards the pile model head. To mitigate rotational effects on the pile model cap induced by lateral load, a steel plate measuring (200 mm x 100 mm) was interposed between the load cell and the pile model cap. Concurrently, two horizontal LVDTs were employed to monitor the lateral displacement. The lateral load, administered by a hydraulic pump connected to the horizontal hydraulic arm, and the resulting displacement were both recorded using the identical data acquisition system as employed in the vertical load and displacement experiments. The overall layout of the experimental configuration for the lateral load tests conducted on the pile models is illustrated in Figure 4b.

Moreover, an array of strain gauges was implemented across various models of CCFAT piles to gauge the bending moment during lateral load testing. It may be stated that CCFAT piles present a viable alternative owing to their inherent stiffness. The selected pile configurations comprised single CCFAT piles with an L_m/D of 10 and 20, facilitating an examination of bending moments across different slenderness ratios within CCFAT piles. Additionally, a 2x2 pile group with a L_m/D of 15 was employed to investigate the bending moment variation within the pile group. The term "pile row" designates piles aligned perpendicular to the direction of lateral load application. Notably, the assumption of identical responses among piles in each row, as posited by Rollins, Peterson and Weaver [36] led to the instrumentation of strain gauges solely on one pile per row. Each individual pile model was equipped with six strain gauges on its outer surface, evenly spaced at vertical intervals from the base as shown in Figure 5. Furthermore, the data acquisition system utilised for strain recording was the 800SM with 8 channels, capturing strains along the embedded length of the pile.

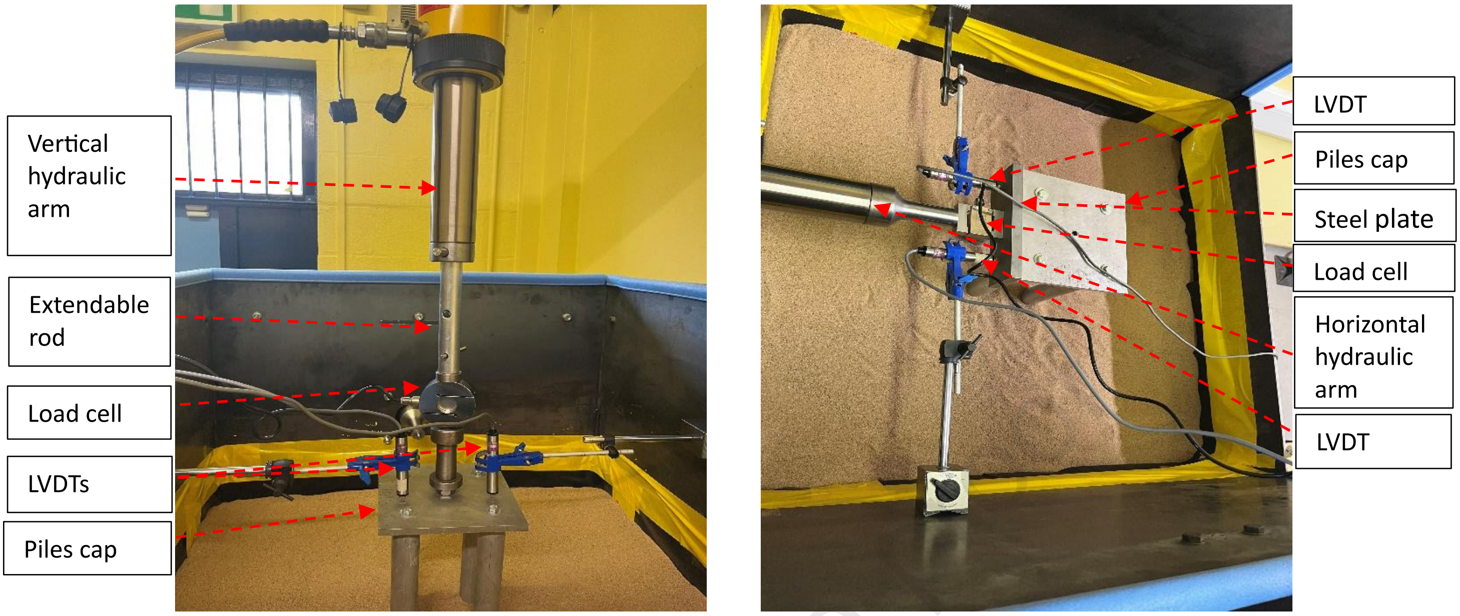

(a) Configuration for vertical load tests (b) Configuration for the lateral load tests

Figure 4. Experimental loads configuration

Figure 5. Strain gauges installation 2x2 CCFAT pile

3. Results and Discussion

3.1. Experimental Investigation

3.1.1. Comparison between CCFAT and traditional pile models

Figure 6a illustrates the variation of vertical load versus settlement of CCFAT, HAT, and PC piles with 2×1 configuration in loose sand conditions (D_r = 30%), for an L_m/D ratio of 10. It is noteworthy that traditional piles achieve ultimate vertical bearing capacity when the vertical load induces a vertical settlement equal to 10% of the diameter of the pile (British Standards Institute, 2020). In this study, the ultimate vertical capacity for all the foundation types has been defined as the settlement that corresponds to 10% of the diameter of the foundation. From Figure 6a, at a smaller magnitude of vertical load, for CCFAT, PC and HAT piles, the settlement is noted to increase almost linearly, beyond which the settlement is noted to increase in a non-linear manner, characterised by a more pronounced slope. The vertical load tests revealed comparable behavior between the CCFAT pile and PC pile models, with both exhibiting similar trends. The ultimate vertical capacities (P_{uv}) for CCFAT, PC and HAT pile models were found to be 781.62, 778.80 and 432.40 N, respectively. Notably, the CCFAT pile model exhibited higher vertical load-carrying capacity when compared with the HAT pile model. The ultimate vertical bearing capacity, obtained for the CCFAT pile is nearly twice the ultimate vertical bearing capacity observed for the HAT pile model. The vertical load-settlement curve shows that the CCFAT pile model exhibited a rapid resistance increase, which can be attributed to the early mobilisation of bearing capacity. This suggests a substantial influence of bearing capacity on the performance of pile foundations under vertical loads. In terms of total vertical load capacity (P_{Tv}), representing the peak load recorded at the termination of vertical load versus vertical settlement curves, the CCFAT, PC and HAT pile models exhibited capacities of 2708.64 N, 2956.80 N and 1674.80 N, respectively. This prolonged duration was chosen to observe the complete behavior of the pile under the substantial vertical settlement and ascertain the total vertical load capacity.

Figure 6(b) depicts the lateral load versus lateral displacement derived obtained from the lateral load test. For various foundations under lateral loads, the ultimate lateral load capacity is defined as the lateral loads corresponding to a pile head lateral displacement of 10% of the diameter of the pile, in accordance with the proposition by Randolph (2003). From figure 6(b), with increasing lateral load values, the response of the pile group undergoes rapid increments during the initial elastic stage, transitioning into the plastic stage after reaching critical points where the slopes of the curves undergo significant changes. Notably, the CCFAT pile model distinguishes itself from both the PC and HAT pile models, showcasing superior lateral load-carrying capacity, potentially attributable to its high stiffness. The aluminium component provides the pile with an exceptional strength-to-weight ratio and serves as a mold for the concrete, while the concrete contributes crucial compressive strength and enhances the overall structural stiffness. The ultimate lateral capacity (P_{ul}) for the CCFAT, HAT, and PC models are obtained obtained as 318.35 N, 126.45 N, and 211.12 N respectively. The CCFAT pile model demonstrated a respective increase of approximately 1.5 times and 2.5 times in the ultimate lateral bearing capacity (P_{ul}) compared to the PC and HAT models, respectively. It is noteworthy that, in this study, the lateral load test extended until the pile head displacement reached approximately 25 mm. This prolonged duration was chosen to observe the complete behavior of the pile under substantial lateral deflection and ascertain the total lateral load capacity (P_{Tl}), which amounted to 474.07 N, 303.44 N, and 400.07 N for the CCFAT, HAT, and PC pile models, respectively. The behavior of piles under lateral loading is conventionally governed by the response of soil and the stiffness of the piles [37-39].

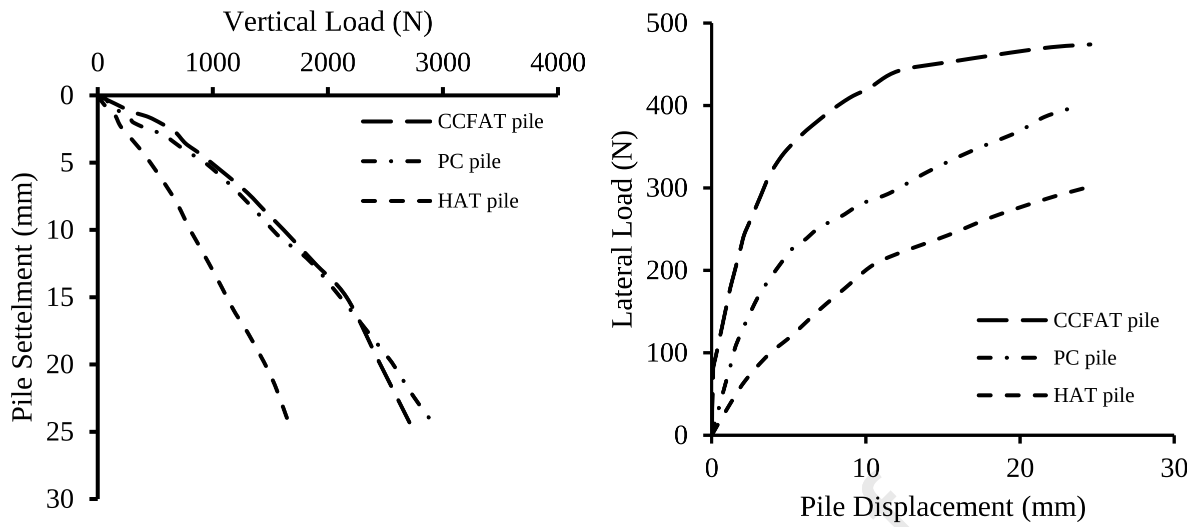

(a) Vertical load versus settlement of 2×1 configuration

(b) Lateral load versus lateral displacement 2×1 configuration

Figure 6. Comparing CCFAT pile and traditional pile models under vertical load

3.1.2. Vertical capacity of CCFAT pile

The application of vertical load testing encompassed CCFAT single, 2x1, and 2x2 pile models, featuring a centre-to-centre spacing equivalent to three pile diameters. The testing protocol incorporated model piles with L_m/D ratios of 10, 15, and 20, with a pile diameter of 38.1 mm shown in Figures 7 (a-c).

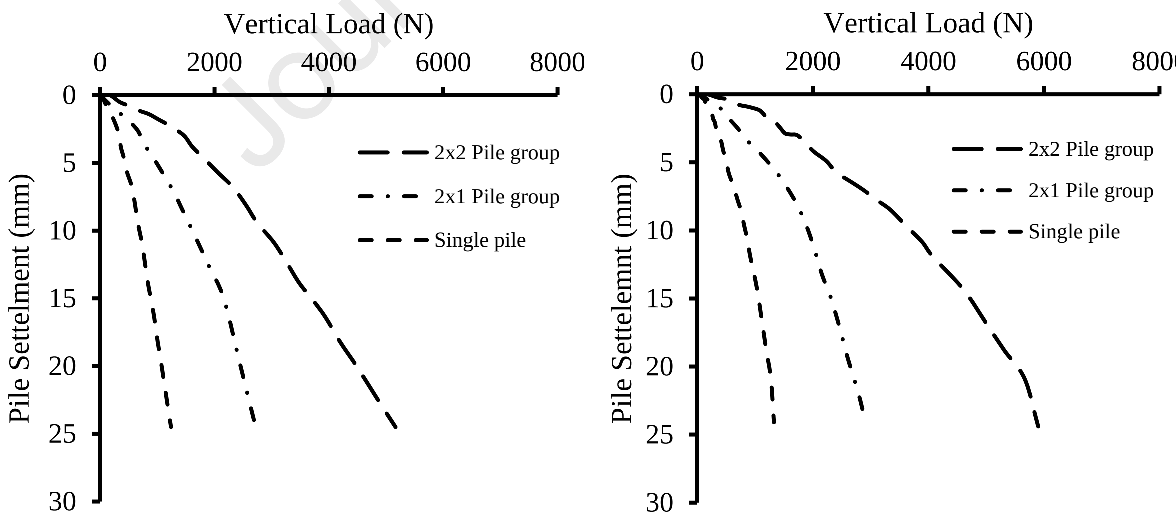

(a) L_m/D =10

(b) L_m/D = 15

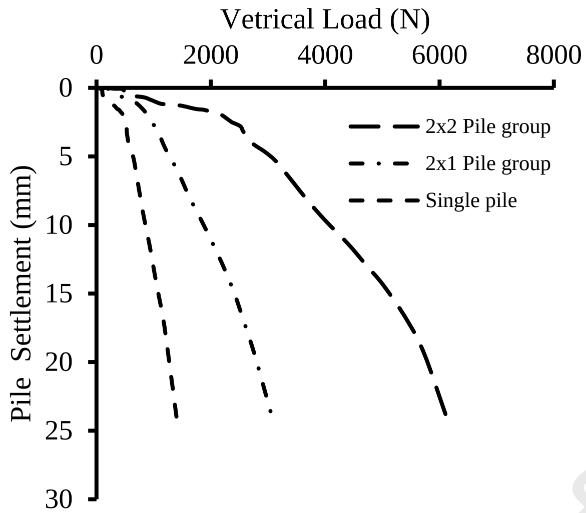

(c) L_m/D = 20

Figure 7. Vertical load versus pile head settlement for CCFAT pile model

The graphical representation in Figure 7 elucidates the relationship between vertical load capacity variation and pile head settlement curves for CCFAT single, 2x1, and 2x2 pile models with L_m/D ratios of 10, 15, and 20.

From Figure 7a, for L_m/D value of 10, the ultimate vertical capacity of a single pile is obtained as 369.88 N. For the same aspect ratio, the ultimate vertical capacities of the 2x1 pile group and 2x2 pile group are obtained as 781.62 and 1611.60 N, respectively. For the same aspect ratio, for single, 2x1 pile group and 2x2 pile group, the total vertical capacities are obtained as 1240.01, 2708.64 and 5166.68 N, respectively. From Figure 7b, for the L_m/D value of 15, the ultimate vertical capacities of single, 2x1 and 2x2 pile groups are obtained as 438.63, 892.17 and 1919.25 N, respectively. For the same aspect ratio, the total vertical bearing capacities are obtained as 1327.72, 2916.47 and 5900.98 N, respectively for single, 2x1 and 2x2 pile groups. The ultimate vertical capacities for L_m/D value of 20 (from Figure 7c) and for single, 2x1 and 2x2 pile groups are obtained as 539.90, 1109.44 and 2562.75 N, respectively. For the same aspect ratios, for single, 2x1 and 2x2 pile groups, the total vertical capacities are obtained as 1419.53, 3102.62 and 6140.61 N, respectively. From the above graph, the maximum ultimate and total vertical capacity is observed for the 2x2 pile group followed by the 2x1 pile group and single pile group.

Notably, a consistent trend is observed across all models, wherein an increase in L_m/D corresponds to an increased vertical capacity. This observed phenomenon is attributed to increased overburden pressure, resulting in an improved mobilised friction resistance developed within the connecting zone of influence in soil-pile interactions. Moreover, the ultimate vertical capacity (P_{uv}) exhibits a noticeable improvement with an increasing number of piles. Importantly, it is noteworthy that the P_{uv} experiences a larger rate of increase with the pile number. The phenomenon of improvement P_{uv} is ascribed to the intensified sand densification occurring during the driving of piles within a larger group, while interaction may cause an opposite effect for the case it seems the densification plays the greater role in increasing the pile to 1X2 and 2x2. To have a better understanding of this phenomenon, the pile group stiffness factor under vertical load (η_V) is introduced. Qu et al. [40] suggested a formal for estimating η_V.

$$\eta_V = \frac{P_{uvg}}{P_{uvs} \times N} \quad (2)$$

In the context of the presented equations, P_{uvg} and P_{uvs} represent the ultimate vertical capacity of the pile group and a single pile, respectively, and N denotes the number of piles within the group. The response of an individual pile within a group differs from that of an isolated pile, especially under vertical loads applied to the shafts. The settlement of one pile in a group induces a settling effect on the adjacent piles, leading to a collective settlement of the group. However, Other studies [41, 42] suggest that η_V is typically estimated based on factors such as pile spacing, soil conditions, the number of piles, and the pile diameter.

The outcomes of the vertical tests for all CCFAT pile models are summarised in Table 2. Notably, the values of η_v surpass 1.0, and there is an observable increase in η_v with a concurrent rise in the number of piles [43]. For instance, in the case of CCFAT 2x1 and 2x2 models with a L_m/D ratio of 10, the η_v values were 1.06 and 1.09, respectively. A comparable trend is observed with other aspect ratios, predominantly contributing to the higher ultimate and overall vertical load capacities.

Table 2. Pile group stiffness CCFAT pile models under vertical loading

Model details	**L_m/D**	**η_V**
Single	10	-
2x1 pile group	10	1.06
2x2 pile group	10	1.09
Single	15	-
2x1 pile group	15	1.02
2x2 pile group	15	1.09
Single	20	-
2x1 pile group	20	1.03
2x2 pile group	20	1.19

3.1.3. Lateral capacity of CCFAT pile

The lateral load testing was conducted on various configurations of CCFAT pile models, including single piles, 2x1 arrangements, and 2x2 configurations. These tests utilized a center-to-center spacing equal to three times the diameter of the piles. Additionally, the experimental setup involved model piles with length-to-diameter ratios (L_m/D) of 10, 15, and 20 with a pile diameter of 38.1 mm.

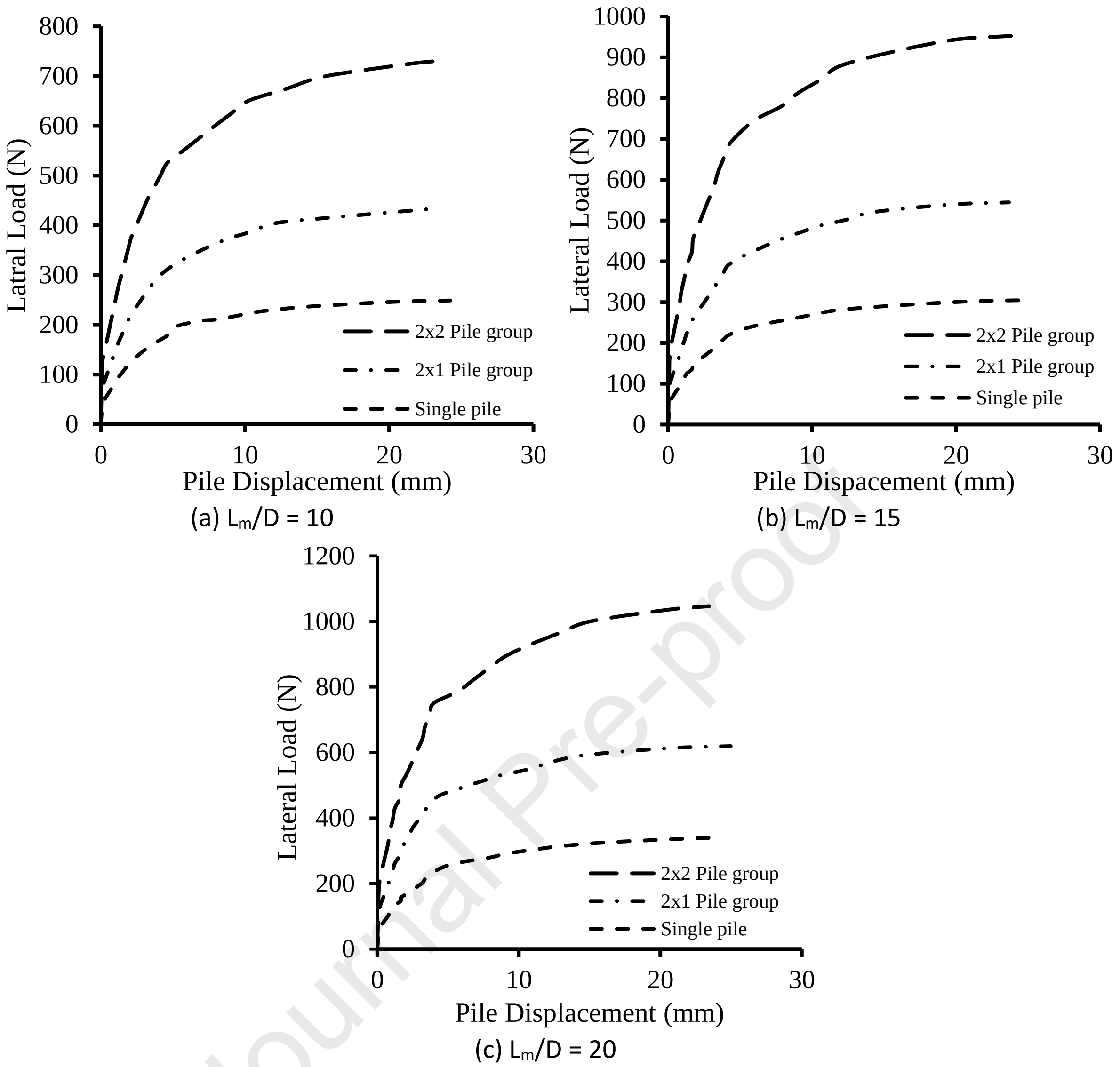

Figure 8. Total lateral load and pile head vertical settlement curves of CCFAT pile model

Figure 8 illustrates the variation of lateral load versus pile head lateral displacement for single, 2×1 and 2×2 pile groups for L_m/D ratios of 10, 15 and 20. For all the geometries considered in the study, the lateral capacity is noted to increase in near-linear maner upto small pile displacement. Beyond a certain limit, the lateral capacity is noted to increase non-linearly up to the ultimate condition. This nonlinear behavior may be ascribed to the likelihood of inelastic dilatancy, causing destabilisation in the strain field and resulting in the localisation of plasticity. The movement of sand particles towards a more stable arrangement during various deformation stages exacerbates the development of plastic strain, as indicated by Li et al. [44].

The variation is noted to be similar for all the configurations and aspect ratios considered in the study. From Figure 8a, the ultimate lateral capacity of a single pile for L_m/D of 10 is obtained as 164.98 N. For the aspect ratio, the ultimate lateral capacity is obtained as 291.77 and 483.86 N, respectively, for 2×1 and 2×2 pile groups, respectively. For the same aspect ratio, the total lateral capacities are obtained as 248.88, 433.73 and 732.00 N, respectively for single, 2×1 and 2×2 pile groups. From Figure 8b, in the case of L_m/D ratio of 15, the ultimate lateral capacities are obtained as 207.16, 369.90 and 646.50 N, for single, 2×1 and 2×2 pile groups, respectively. For the same aspect ratio, the total lateral capacities are obtained as 304.75, 544.46 and 952.33 for single, 2×1 and 2×2 pile groups, respectively. For L_m/D

of 20 (from Figure 8c), for single, 2×1 and 2×2 pile groups, the ultimate lateral capacities are obtained as 230.82, 439.77 and 743.76 N, respectively. From the same figure (8c), the total lateral capacities of L_m/D are obtained as 340.20, 619.38 and 1046.76 N, respectively, for single, 2×1 and 2×2 pile groups. From the study, the maximum ultimate and total capacities are obtained for 2×2 pile group followed by 2×1 pile group and single pile.

In the examination of the influence of L_m/D, it was observed that, for the same number of piles, models with longer pile conditions tend to exhibit a larger ultimate capacity compared to those with shorter pile conditions, and the initial stiffness was generally improved. This phenomenon can be attributed to the increase in passive resistance with the elongation of pile length. While the ultimate lateral capacity (P_{ul}) was significantly enhanced with an increase in the number of piles, this enhancement occurs at an increasing rate. This observation is likely due to the influence of pile shadowing within the pile group [20]. The presence of neighbouring piles reduces the soil resistance applied to individual piles, leading to an overlap of failure zones as piles move laterally under external loads. Consequently, the surrounding soil loses portions of its resistance, resulting in a diminished lateral capacity compared to the situation with a single pile, as elucidated by Gao and Zhao [45].

To delve further into these effects, the pile group stiffness factor under lateral load (η_l) is introduced, with its estimation following the methodology proposed by Wang, Li and Li [20] .

$$\eta_l = \frac{P_{ulg}}{P_{uls} \times N} \tag{3}$$

In the context of the equations presented, P_{ulg} and P_{uls} represent the ultimate lateral capacity of the pile group and a single pile, respectively, while N denotes the number of piles within the group. The outcomes of the lateral tests for all CCFAT pile models are summarised in Table 3. It is noteworthy that the values of η_l were below 1.0, and there was an observed decreasing rate with the increase in the number of piles. For instance, in the case of CCFAT 2x1 and 2x2 models with a L_m/D ratio of 10, the η_l values were 0.88 and 0.73, respectively.

Table 3. Experimental tests for all CCFAT pile models under lateral loading

CCFAT pile model	**(L_m/D)**	**η_l**
Single	10	-
2x1 pile group	10	0.88
2x2 pile group	10	0.73
Single	15	-
2x1 pile group	15	0.89
2x2 pile group	15	0.78
Single	20	-
2x1 pile group	20	0.95
2x2 pile group	20	0.81

3.1.4. Bending moment along the embedment length

The calculation of the bending moment along each distinct instrumented pile model is achievable through analysis of the readings obtained from the strain gauges strategically positioned along the embedded length of the pile model. In accordance with the principles elucidated in the theory of elasticity and Hooke's law [46], the induced moment within the pile section is functionally linked to the measured strain values recorded by the strain gauges, as denoted by the following equation:

$$M = (EI)p\frac{\epsilon}{r} \tag{4}$$

$$(EI)p \text{ for CCFAT piles} = E_aI_a + K_e \times (E_cI_c) \tag{5}$$

Herein, E_a and E_c denote the modulus of elasticity for the aluminium tube and concrete infill, respectively, while I_a and I_c represent the moment of inertia pertaining to the aluminium tube and concrete infill, respectively. K_e is denoted as the correction factor for concrete and is equal to 0.6 [23, 47].

Ec can be calculated as:[23, 48]

$$Ec\ = 22000\left(\frac{fc+8}{10}\right)^{0.3} \tag{6}$$

Here, fc is the concrete cube compressive strength=30MPa.

The variable ϵ is defined as the peak recorded strain observed in the strain gauges, and ' r ' signifies the outer radius of the CCFAT pile.

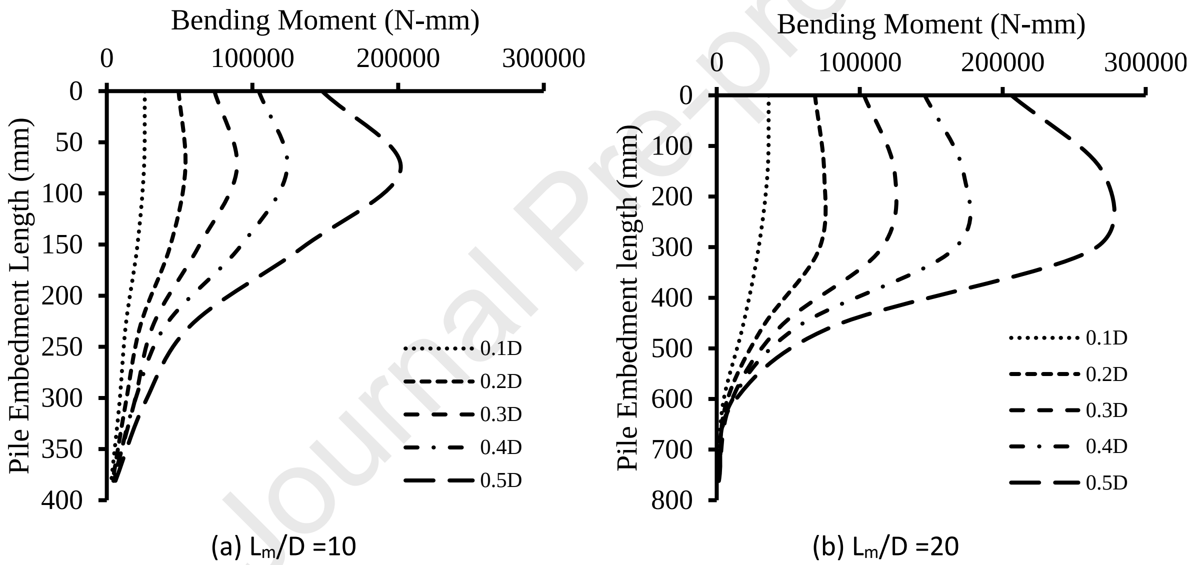

Figure 9. Bending moment profile for single CCFAT pile

Figure 9 (a and b) illustrates the evolution of the bending moment profile in response to pile head displacement for a singular CCFAT pile, with respective aspect ratios of 10 and 20. The bending moment exhibits a consistent upward trend with increasing applied load across all scenarios. Notably, the bending moment values were maximum at the midline level, followed by a gradual decrease with depth in a parabolic manner along with embedment length.

From Figure 9(a), for L_m/D ratio of 10, the lateral loads were applied corresponding to 0.1, 0.2, 0.3, 0.4 and 0.5 times the diameter of the pile (D) and the corresponding bending moment variation along the embedment depth has been recorded. The maximum bending moments for a single CCFAT pile, obtained at the mud line for 0.1D, 0.2D, 0.3D, 0.4D and 0.5D are 26086.07, 93512.02, 73912.54, 104347.11 and 147825.08 N-mm, respectively. From Figure 9(b), for the same pile configuration, as the L_m/D value is increased to 20, the maximum bending moments obtained at the mud line level are 36363.38, 75151.01, 124443.59, 145453.55 and 206059.19 N-mm, respectively, for lateral loads applied corresponding to 0.1, 0.2, 0.3, 0.4 and 0.5 times the pile diameter.

It was noteworthy that, at equivalent pile head displacements, the pile characterised by L_m/D of 20 demonstrates superior resistance to bending moment compared to its L_m/D of 10 counterparts. This difference can be ascribed to the fact that the pile with L_m/D of 10 exhibits substantially lower load resistance than the pile group with L_m/D of 20, at identical pile head displacements. Furthermore, in the case of the L_m/D of 20, there is a marginal increase in the depth at which the maximum bending moment occurs throughout the loading process, while this depth remains constant for the L_m/D value of 10 model. This phenomenon may be attributed to the persistence of pile stiffness dependency as specific parameters, even in the face of soil degradation surrounding the pile, influencing the determination of the maximum bending moment [49, 50].

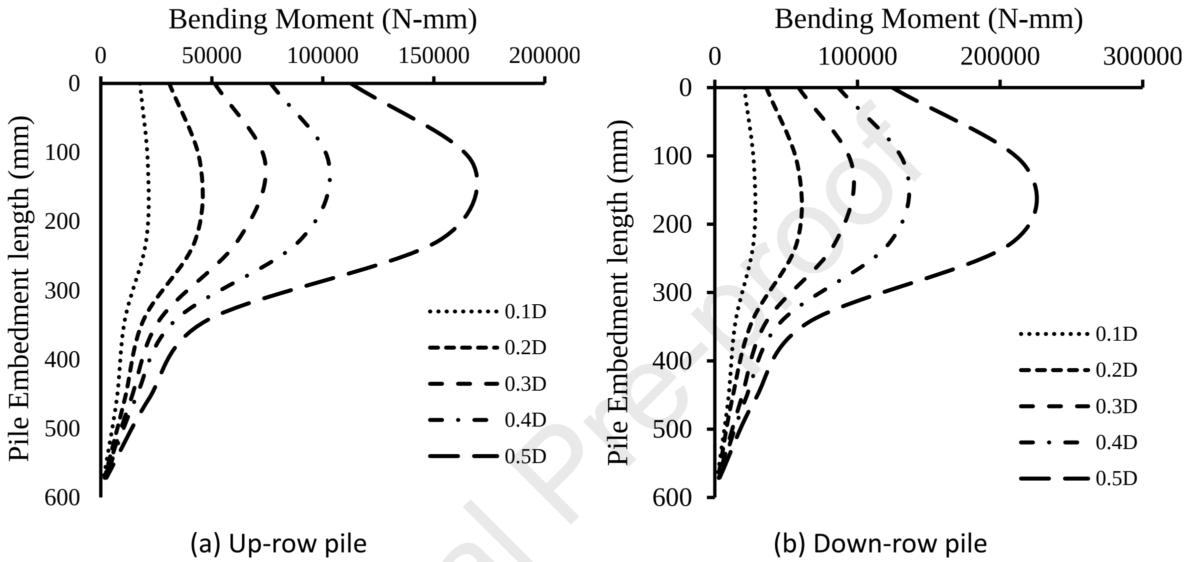

Figure 10. Bending moment profile for 2x2 CCFAT pile group with L_m/D = 15

Figure 10 (a-b) depicts the progress of the bending moment profile concerning pile head displacement for both up-row and down-row piles within a 2x2 pile group, which is characterised by an aspect ratio of 15. The observed trend mirrors that of a single pile, with the bending moment escalating with the applied load. However, noteworthy distinctions emerge in the bending moment profiles between up-row and down-row piles, where the down-row pile consistently exhibits greater resistance to bending moment than its up-row counterpart. For example, from Figure 10a, for up-row pile, the maximum bending moment obtained at the midline for lateral load corresponding to 0.1D, 0.2D, 0.3D, 0.4D and 0.5D are 21155.41, 44717.84, 51302.61, 76544.86 and 112605.22 N-mm. For the same geometry and aspect ratio, from Figure 10b, for 20624.37, 36116.04, 58690.19, 86572.24 and 124428.77 N-mm, respectively, for applied lateral load corresponding to 0.1D, 0.2D, 0.3D, 0.4D and 0.5D.

This variation in bending moment response can be attributed to, firstly, the up-row pile experiencing tension, while the down-row pile undergoes compression. This distinction results in a multiplication effect of the vertical load by the horizontal displacement, influencing the magnitude of the bending moment [16, 51]. Secondly, the up-row pile falls within the active zone of the down-row pile, thereby experiencing a shadowing influence [38, 52]. While the maximum bending moment was achieved at nearly identical positions for both up-row and down-row piles. Despite these variations, there was no discernible movement in the depth at which the maximum bending moment occurs for both up-row and down-row piles. This observation underscores the significance of pile stiffness in shaping the bending moment profile, as stiffness remains a consistent factor influencing the characteristics of the bending moment.

3.2. Finite Element Analysis

Alongside the experimental investigation, computational analyses were conducted using finite element software ABAQUS [53], to gain deeper insights into the vertical and lateral responses and load transfer mechanism of CCFAT pile groups. The results of experimental tests were compared with those of results obtained from numerical simulations. Subsequent to the confirmation of model validity, a parametric investigation was executed, with the objective of investigating supplementary performance data across diverse configurations of CCFAT pile groups. Additionally, sensitivity analysis was performed, encompassing variations in both soil properties and the coefficient of friction between CCFAT piles and the surrounding soil. The forthcoming sections expound upon the simulations, methodologies employed, and precision of the finite element models, as well as the details of the parametric and sensitivity analyses.

3.2.1. Simulation Details

The simulation activities encompassed the modelling of CCFAT pile groups, specifically 2x2 configurations with a L_m/D of 10, 2x1 configurations with a L_m/D of 20, and individual piles with a L_m/D of 15. These configurations were selected for the purpose of validating the experimental investigation. Furthermore, a parametric study was conducted to explore novel CCFAT pile group configurations with an L_m/D of 15, namely 2x3 and 3x3, in addition to single configurations, 2x1, and 2x2 with an L_m/D of 15.

Considering the geometric and loading symmetry, only half of the entire soil domain and the CCFAT pile geometries were modelled. The dimensions of the simulated soil domain corresponded to half of the area of the soil chamber employed in the experimental test for the validation study. Conversely, for the novel configurations, the extent of the soil domain was determined to mitigate boundary effects. The finite element mesh, illustrated in Figure 11, shows the discretised representation of the simulated section, including the soil domain, the CCFAT pile group (2x1) having L_m/D value of 15, and the assembly of these piles embedded in the soil domain. The soil domain, aluminium tube, and concrete component were simulated using first-order, eight-node linear brick elements with reduced integration (C3D8R). Due to its single integration point, the C3D8R element avoids numerical instabilities and has been widely and successfully used for modelling composite structural members and addressing geotechnical problems [3, 35]. To optimise computational accuracy and efficiency, finer meshing was applied near the pile models and the ground surface, while coarser meshes were employed in regions farther away from the piles. Boundary conditions were implemented by restraining the bottom boundary of the soil domain in all directions, while the vertical boundaries were constrained in the horizontal direction. Additionally, normal displacements were constrained within the symmetric plane.

The behavior of the loose sand bed was simulated using the Mohr-Coulomb (M-C) elastoplastic constitutive model with a non-associated flow rule. The M-C model has been chosen because it strikes a good balance between simplicity, computational efficiency, and accuracy for a range of geotechnical problems. The soil properties were measured from the laboratory tests and calibrated with several numerical models [54-56] are presented in Table 4. After the engineering stress and strain for the aluminium obtained from the coupon tests were converted to true stress and logarithmic plastic strain. The aluminium tube and pile cap were simulated as elastic-plastic with Young's modulus of 70 GPa, Poisson's ratio of 0.3, and density of 27 kN/m^3. For concrete compounds, a linear elasticity model was applied with Young's modulus of 25 GPa, Poisson's ratio of 0.16, and a density of 24 kN/m^3.

In ABAQUS, one available option for modelling contact between the soil and foundation, or between composite elements, is the surface-to-surface approach, which has been employed in numerous studies [23, 52]. This method utilizes the master-slave concept, wherein the master surface is stiffer than the slave surface. Typically, the master surface is more finely discretized than the slave surface and may penetrate the latter, depending on the type of discretization applied in the analysis. In this study, to facilitate a realistic representation of interactions, a surface-to-surface contact approach was implemented to simulate the contact between the soil and the external surface of the CCFAT pile model, as well as the contact between the inner surface of the aluminium tube and the outer surface of the concrete compound. Specifically, the contact was defined with the outer surface of the aluminium tube serving as the master and the soil surface as the slave. Conversely, for the contact between the aluminium tube and the concrete compound, the outer surface of the concrete compound was designated as the master, while the inner surface of the aluminium tube acted as the slave. The interface governing these interactions was modelled using the "hard" contact model with Coulomb's tangent friction, with a specified friction coefficient between the CCFAT pile and soil assumed to be 0.3 [18, 23, 57, 58]. The hard contact relationship was used in the normal direction to account for the development of normal stresses between surfaces without penetration between aluminum tube-concrete interface. However, when considering the contact between the aluminum tube and soil, significant undetected penetration of the master surface into the slave surface has been observed.

To emulate the experimental test conditions, the application of loads occurred in two sequential steps. In the initial step, a geostatic load was applied to establish the initial stress state across the entire soil domain. Subsequently, in the second step, loads were applied individually to the reference point at the pile cap for both vertical and lateral load tests. The load conditions were simulated using a displacement control method, ensuring a controlled and representative loading scenario.

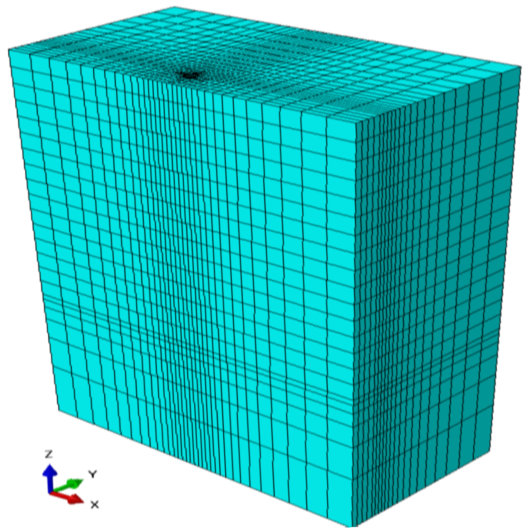

(a) Soil domain mesh

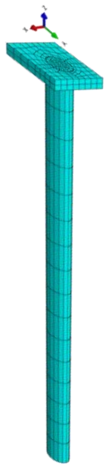

(b) CCFAT pile group mesh

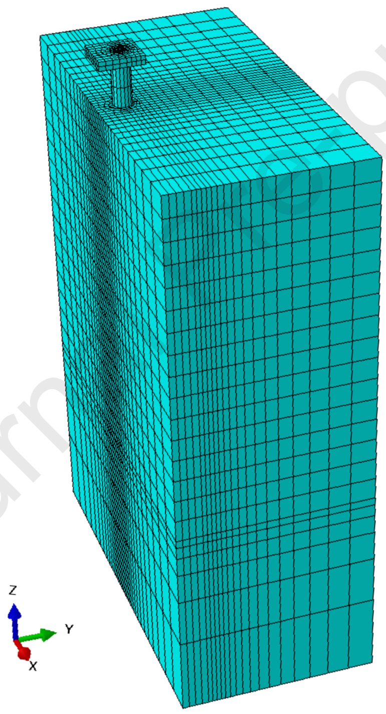

(c) Assembly mesh

Figure 11. Finite element meshes for CCFAT pile group (2x1), with (L_m/D) 15

Table 4. The loose sand properties

Soil parameter	Value
Young's modulus, E (MPa)	20
Poisson's ratio, μ	0.2
Density, γ (kN/m^3)	16.06
Internal friction angle, Φ (^{o})	30
Dilatancy angle, ψ (^{o})	5

3.2.2. Validation of the FEM models

To ensure the appropriateness of finite element (FE) simulation steps, for validation, the results obtained from the finite element simulation were compared with experimental results, carried out on three CCFAT pile models, subjected to vertical and lateral loading. The selected pile models included a single pile with an L_m/D of 15, a 2x1 configuration with an L_m/D of 20, and a 2x2 configuration with an L_m/D of 12. The chosen models exhibited variations in pile configuration and L_m/D. Figure 12a and Figure 12b presents a comparison between the vertical load versus vertical settlement curves and lateral load versus lateral displacement curves, respectively, obtained from laboratory experiments and FE simulations.

The figures depict the correspondence of behavioral responses between the experimental and FE results concerning the vertical and lateral aspects of the CCFAT pile models. In both loading scenarios, the FE model successfully captures the general trends observed in the experimental tests. However, the calculated FE curves exhibit smoother profiles compared to the experimental test curves. It was noteworthy that the stiffness of the FE simulation was marginally lower than that observed in the experimental tests. This discrepancy may be attributed to the simplifications employed in the simulation approach, particularly in representing the contact between the soil and both the outer surface of the CCFAT pile model and the inner aluminium surface of the concrete compound. Such simplifications aimed to address the inherent complexities of real-world scenarios involving composite piles in soil. Other factors collectively explain why the finite element model's results might differ from the experimental test results, especially for complex composite pile-soil interactions. Such as i) the boundary conditions applied to represent the far-field soil may differ from experimental test conditions. In tests, the boundary effects can play a significant role. ii) The accuracy of finite element results depends on the mesh quality. A coarse or poorly refined mesh may not capture the stress concentrations or local failure mechanisms around the pile, which can lead to deviations when compared to experimental test results.

Furthermore, a satisfactory agreement was observed between the experimental tests and FE simulations in terms of total load capacity for both vertical and lateral loading, denoted as (P_{Tv}) and (P_{Tl}). Table 5 provides the ratios of capacities obtained from experimental to FE simulation values for total vertical load capacities ($P_{Tv,Exp.}$/ $P_{Tv,FE}$) and total lateral load capacities ($P_{Tl,Exp.}$/ $P_{Tl,FE}$). The ratios were found to be close to unity, with the single CCFAT pile model yielding the most accurate predictions of load capacity. Specifically, the values for ($P_{Tv,Exp.}$/ $P_{Tv,FE}$) and ($P_{Tl,Exp.}$/ $P_{Tl,FE}$) were determined to be 1.02 and 1.01, respectively.

In summary, the developed FE models demonstrated the capability to predict the behavioral responses of CCFAT pile models under both vertical and lateral loading conditions in loose sand with reasonable accuracy.

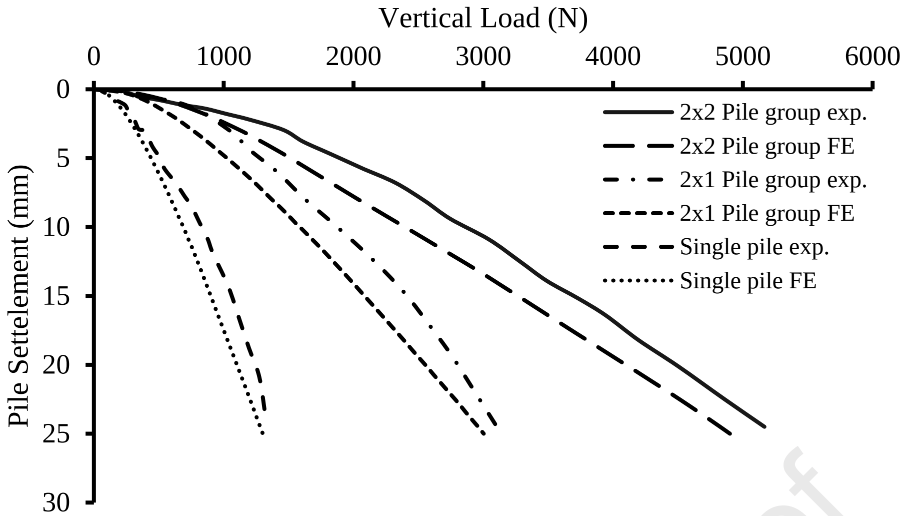

(a) Vertical load versus settlement response

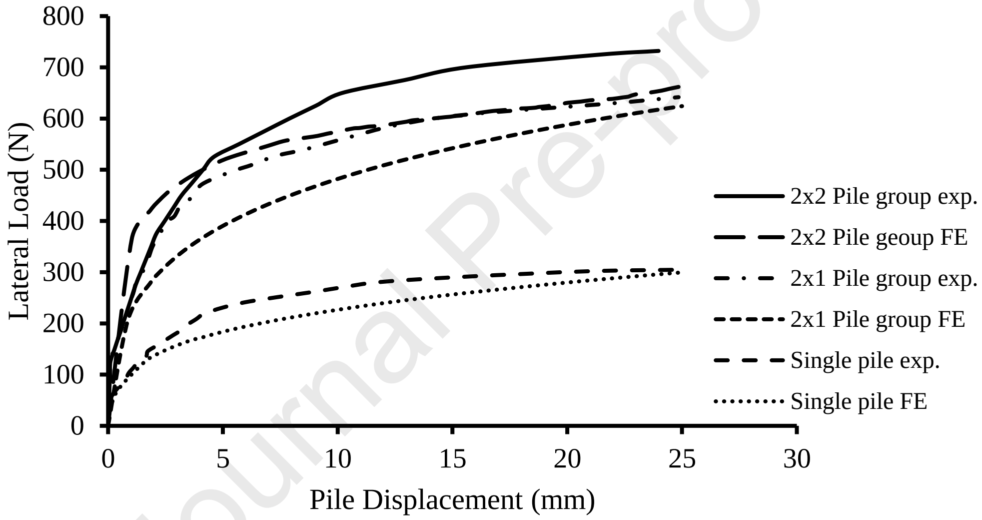

(b) Lateral load versus lateral displacement response

Figure 12. Comparison of experimental and FE results

Table 5. Comparison of experimental and FE values for total vertical and lateral load capacities

Model details	**L_m/D**	**$P_{Tv,Exp.}/P_{Tv,FE}$**	**$P_{Tl,Exp.}/P_{Tl,FE}$**
Single	15	1.02	1.01
2x2 pile group	10	1.04	1.03
2x1 pile group	20	1.06	1.10

3.2.3. Vertical load and lateral capacities of CCFAT piles

The experimental examinations conducted in this investigation primarily focus on comparing the CCFAT pile model with traditional pile models. The study evaluates the behavioral response of CCFAT piles under both vertical and lateral loading cases, with emphasis on the bending moment along the embed length. A novel configuration of CCFAT pile groups was thoroughly examined, leveraging finite element (FE) simulations to explore the wide range of possible spaces. The parametric study involves a series of validated FE models, considering various CCFAT pile configurations, including single, 2x1, 2x2, 2x3, and 3x3 arrangements. The number of piles was identified as a critical parameter influencing the vertical and lateral bearing capacity of the pile group [54, 59]. To mitigate the boundary effect in simulations for 2x3 and 3x3 configurations, multiple attempts were made to increase the width of the soil domain in the direction of lateral load application. The width was set to 1200 mm, differing from the 900 mm used in other model configurations. The length of the soil domain remains consistent at 1200 mm, as the vertical behavior is unaffected by changes in length.

The application of vertical and lateral loads obtained from the FE parametric study covers CCFAT single, 2x1, 2x2, 2x3, and 3x3 pile models, featuring a centre-to-centre spacing equivalent to three pile diameters and a L_m/D of 15. This ratio is chosen based on the validation of the CCFAT single model through experimental tests under both vertical and lateral loading conditions.

Figure 13 provides a graphical representation, elucidating the relationship between total vertical load and pile head vertical settlement curves for selected CCFAT pile models. The vertical capacity of the pile groups exhibits a continuous increase with the pile number, however, notable differences in the stiffness were observed. Models 2x1 and 2x2 exhibited stiffer responses compared to models 2x3 and 3x3, indicating distinct patterns in vertical capacity increase with varying pile numbers.

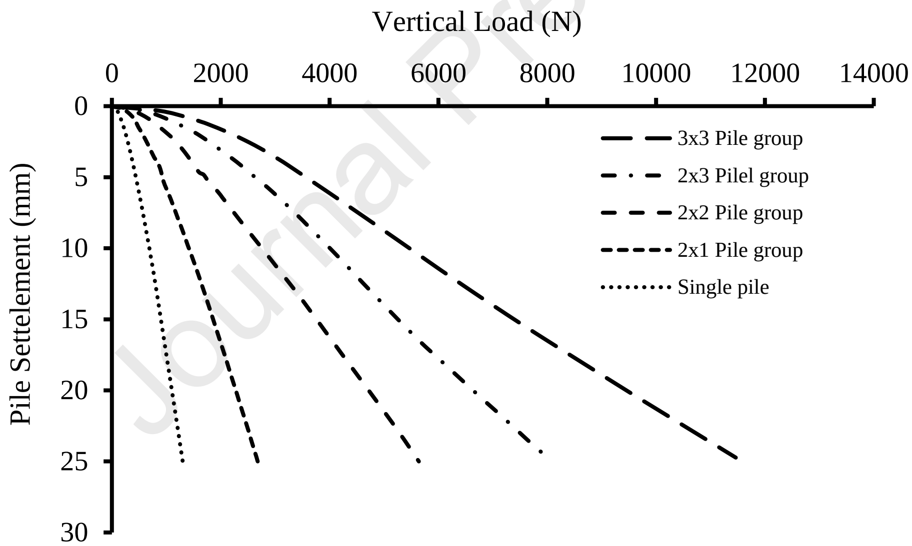

Figure 13. Vertical load vs pile head vertical settlement curves for different CCFAT pile models

From figure 13, pile settlement for various CCFAT geometries considered in this study is noted to increase with applied vertical load. The ultimate vertical and total vertical capacities are noted to be maximum for the 3×3 CCFAT pile group followed by 2×3, 2×2, 2×1 and single pile configurations, respectively. For instance, for the 3x3 pile group, the ultimate vertical and total capacities are obtained as 3101.38 and 11579.9 N, respectively. The ultimate and total vertical capacities have been noted to decrease to 2494.30 and 8083.10 N, respectively for the 2x3 pile group. The ultimate and total vertical capacities have been further noted to reduce to 1792.84 and 5640.59 N, respectively, for the 2x2 pile group. For the 2x1 pile group, the ultimate vertical and total capacities are obtained as 865.33 and 2679.15 N, respectively. For single pile group, the ultimate and total vertical capacities are obtained as 426.19 and 1300.59 N, respectively.

The increase in vertical capacity for higher numbers of piles in the groups can be attributed to several factors. As more piles are added, the load from the applied is distributed across a greater number of piles, reducing the load per pile and allowing each to perform more efficiently. Additionally, the combined surface area in contact with the soil increases, enhancing skin friction and overall load-bearing capacity. The interaction between piles in a group also contributes to improved load sharing and stabilization of the surrounding soil. This collective action reduces settlement, thereby increasing the perceived vertical capacity.

To facilitate the understanding of the comparison, Table 6 presents the calculated values η_v for the FE simulation under vertical load. Notably, η_v values exceed 1.0 for models 2x1 and 2x2, suggesting a larger rate of increase in P_{uv} with the pile number compared to experimental observations. Conversely, models 2x3 and 3x3 exhibit η_v values under 1.0, indicating a larger rate of decrease in P_{uv} with increasing pile number. These observations may be attributed to densification during pile driving within larger groups, with significant effects observed up to four piles in the group. Beyond this point, negative pile interaction becomes a significant factor, surpassing the benefits of the densification process.

Table 6. FE Results for CCFAT pile models under vertical loading

CCFAT pile model	$\boldsymbol{\eta_v}$
Single	-
2x1 pile group	1.015
2x2 pile group	1.052
2x3 pile group	0.980
3x3 pile group	0.810

Figure 14 depicts the variation of lateral load capacity with pile head lateral displacement for single, 2x1, 2x2, 2x3, and 3x3 pile models having L_m/D of 15. The lateral capacity exhibited enhancement with an increasing pile number; however, the rate of improvement in the lateral capacity was less than the lateral capacity of the single pile model, multiplied by the number of piles. This phenomenon underscores the influence of the shadowing effect, wherein the internal soil fails to provide full resistance due to the presence of neighbouring piles. The ultimate and total lateral capacities are highest for the 3x3 pile group, followed by the 2x3, 2x2, 2x1, and single pile configurations. For example, the ultimate and total lateral capacities obtained for the 3x3 pile group are 1146.96 and 1603.30 N, respectively. For the 2x3 pile group, the ultimate and total lateral capacities are noted to reduce to 805.81 and 1195.88 N, respectively. In the case of the 2x2 pile group, the ultimate and total lateral capacities are further noted to reduce to 540.01 and 922.77 N, respectively. The ultimate and total lateral capacities for the 2x1 pile group are obtained as 301.64 and 510.47 N, respectively. For single pile, the ultimate and total lateral capacities are found as 184.26 and 300.00 N, respectively.

As compared to single pile, the applied lateral loads in pile groups are distributed among all the piles, which reduces the load on each individual pile and improves the ability of the pile group to withstand greater lateral forces. With the increasing number of piles in the group, the interaction between the piles and the surrounding soil is increased due to increasing surface area, thereby enhancing the lateral resistance of group piles as compared to isolated piles.

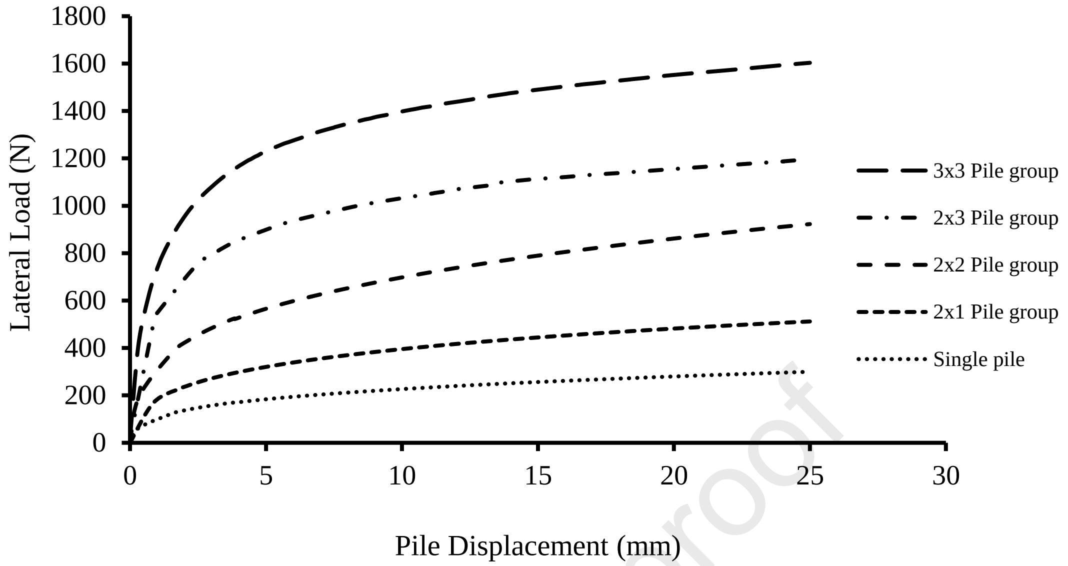

Figure 14. Lateral load vs pile displacement curves for different CCFAT pile models

The stiffness of the pile group subjected to lateral load is determined using Eq. (3) and the values are listed in Table 7. From the table, the lateral load transfer ratio (η_l) is noted to decrease with increasing number of piles. The decrease in pile group stiffness with the addition of piles under lateral load can be attributed to several factors. overlapped stress zones during the interaction between the piles and the surrounding soil and is discussed further.

Table 7. FE Results for CCFAT pile models under Lateral loading

CCFAT pile model	**η_l**
Single	-
2x1 pile group	0.820
2x2 pile group	0.730
2x3 pile group	0.720
3x3 pile group	0.690

The anticipation ultimate load of the pile under vertical and lateral loading, according to the concepts of geotechnical engineering, becomes feasible by considering the charts pertaining to the pile group stiffness factors (η_v) and (η_l) with the number of piles subjected to both vertical and lateral loading. Pile group stiffness charts play a pivotal role in engineering practice, widely employed in the computation of ultimate and total load for piles and foundations in geotechnical problem-solving [60-62].

The vertical pile group stiffness(η_v) and lateral pile group stiffness (η_l), obtained from the numerical simulation for 2x1, 2x2, 2x3 and 3x3 pile groups are plotted against the number of piles, shown in Figure 15. The data points obtained were used to fit curves and expressions and the general form is given by Eq. 7. that can determine the vertical and lateral stiffness of the pile group, taking into account the effect of the number of piles in the group. Initial estimates for the model parameters were derived from prior experience, and the Least Squares Method was utilized to minimize the discrepancies between the observed and predicted values. The fit was subsequently assessed using residual analysis and metrics such as R-squared and RMSE. Once satisfactory R-squared and RMSE values were achieved, the coefficients of the mathematical models were reported in Table 8.

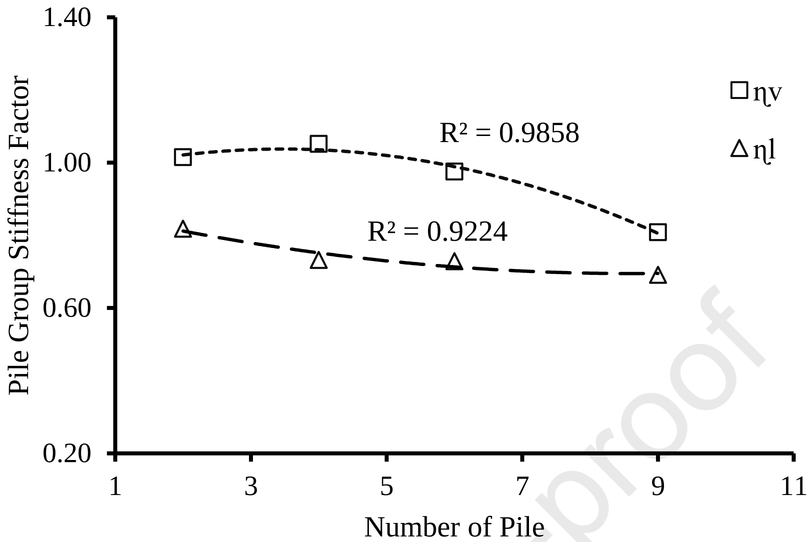

Figure 15. Pile group stiffness chart

$$\eta_v, \eta_l = an^2 + bn + c \tag{7}$$

Where n represents the number of piles and the values of co-efficients to determine η_v and η_l are presented in Table 8.

Table 8. Coefficients to determine η_v and η_l

Coefficients	a	b	c
η_v	-0.0076	0.0528	0.9459
η_l	0.0027	-0.0461	0.8932

This above expression can serve as an initial guideline for the practitioners and designers for designing the CCFAT pile group foundations with the range of geometries and soil parameters considered in this study.

3.2.4. Load transfer mechanism

To further comprehend the load transfer mechanism of vertical load in the soil domain, Figure 16 (a-c) illustrates vertical settlement contours for CCFAT pile groups 2x2, 2x3, and 3x3, respectively. From Figure 16a, under the application of vertical load until failure, a significant downward movement of the soil mass is observed, starting from the mid-depth along the interior and exterior sides of the piles in the group. As the vertical load is increased, the extent of soil movement along the individual piles, from their mid-depth down to the pile tips, is noted to increase progressively. This downward soil movement is most pronounced at the tips of the 2x2 CCFAT pile group, where the maximum settlement of the soil under the vertical load is observed. However, the soil settlement was noted to extend downward only to a certain depth, while the soil mass entrapped within the two piles in the group underwent minimal settlement along the embedded length of the pile group.

From Figure 16b, for the 2x3 CCFAT pile group, a similar soil settlement pattern was observed as in the 2x2 CCFAT pile group, where the soil settlement was noted to propagate from approximately the mid-depth of the piles towards their tips, along both the interior and exterior sides, adjacent to the piles. The maximum settlement was observed at the three pile tips within the group, and considerable soil settlement was also observed down to a certain depth below the tips of the foundation. In contrast to the 2x2 CCFAT pile group, considering the tip level as a reference, a considerably higher extent of downward movement of soil was observed. Furthermore, the soil mass entrapped within the pile group was noted to settle considerably, along with the overall pile group, under the applied vertical load, indicating a block failure mechanism for the pile group foundation.

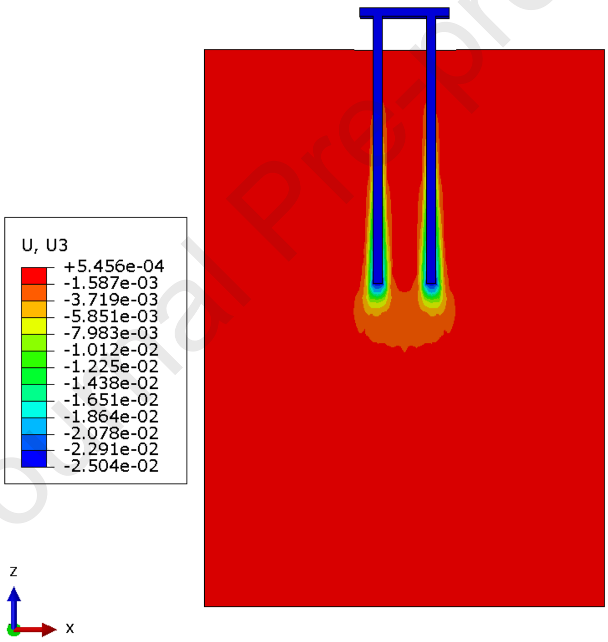

(a) 2x2 CCFAT pile group

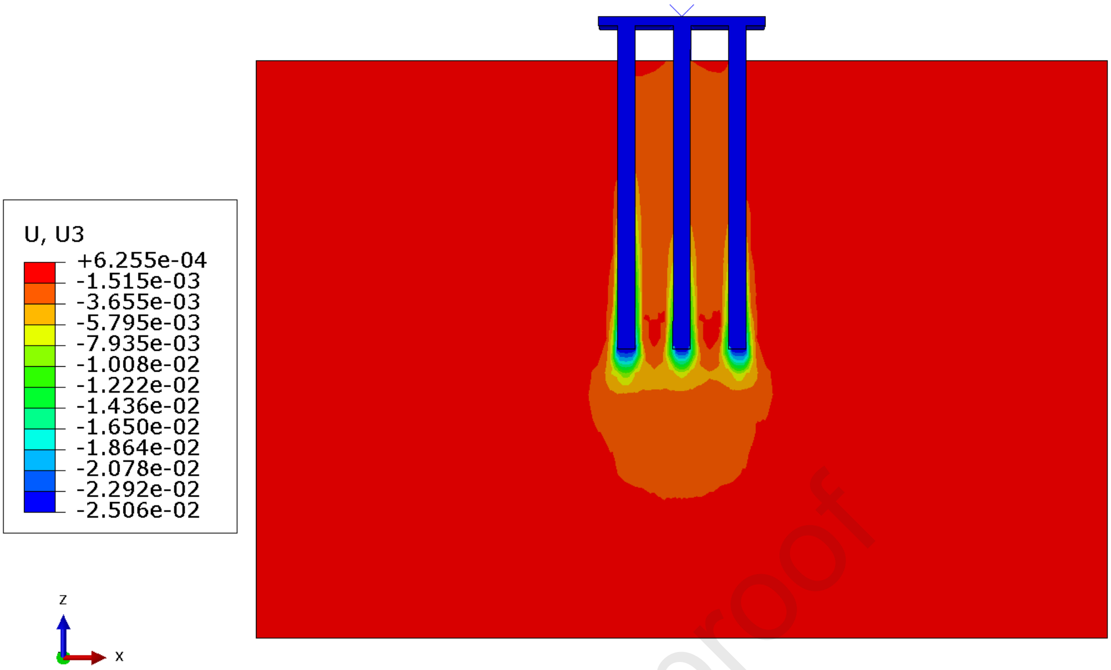

(b) 2x3 CCFAT pile group

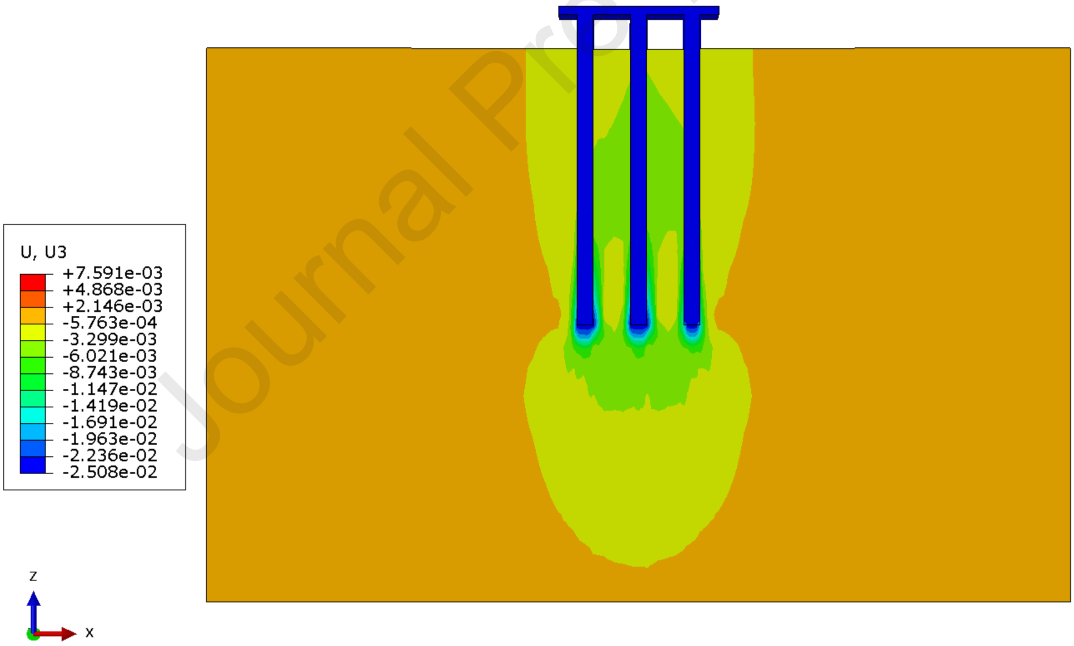

(c) 3x3 CCFAT pile group

Figure 16. Vertical settlement contours for CCFAT pile group under vertical loading

From Figure 16c, in contrast to the 2x2 and 2x3 CCFAT pile groups, the 3x3 CCFAT pile group exhibited a distinct block failure mechanism accompanied by a larger extent of soil deformation towards the right and left sides of the foundation at the bed level, indicating a more pronounced soil movement compared to the smaller pile group configurations. Additionally, a larger extent of soil settlement was also noted below the pile tips within the 3x3 pile group, further highlighting the differences in the soil-pile interaction and overall foundation behavior.

Figures 17 (a-c) present lateral displacement contours for CCFAT pile models arranged in single, 2x3, and 3x3 rows, respectively, in the direction of applied lateral load. Under the application of lateral load until failure, the pile group configurations are observed to undergo a rigid rotation around a specific point along their depth. Above this rotation point, the pile group moves to the right, while below the rotation point, it moves to the left from its initial position, aligning with the direction of the applied lateral load.

Above the rotation point, the rightward lateral displacement of the pile group causes compression in the soil on the right side of the foundation and tension in the soil on the left side, at the bed level. The maximum lateral soil movement occurs at the bed level, on both the compressive (right) and tensile (left) sides of the foundation. The soil displacement along the depth of the extreme left and right piles gradually decreases towards the tips, forming wedge-shaped zones of compression and tension. At the bed level, a significant heave formation is observed on the compressive (right) side of the foundation, while a depressed zone forms on the tensile (left) side.

From the comparison of Figures 17 (a-c), At the bed level, at the point of failure, the single pile group configuration exhibited a relatively lesser extent of soil displacement along the lateral direction, compared to the 2x3 and 3x3 CCFAT pile groups. This suggests a more localized soil deformation pattern for the single pile group, in contrast to the larger 2x3 and 3x3 CCFAT pile groups.

As shown in Figures 17 (b-c), for both the 2x3 and 3x3 CCFAT pile groups, the piles located at the extreme left of the group were noted to move upward, experiencing tensile forces, while the piles at the extreme right side of the group experienced compression, thereby penetrating deeper from their installed position. Additionally, for both the 2x3 and 3x3 CCFAT pile groups, a heave formation was observed at the bed level at failure for the soil mass entrapped within the pile groups.

From the Figure 17(a-c), as compared to a single pile, the 3x3 and 2x2 CCFAT pile groups underwent rigid rotation and experienced differential movement of the pile group, which allows for the engagement of more soil zone and mobilization of higher lateral resistance. The formation of soil compression and tension zones, along with wedge-shaped deformation patterns and heave/depression formation at the bed level, contributes to the increased lateral capacity of the pile groups. In contrast, the single pile group exhibits a more localized soil deformation pattern, resulting in lower lateral capacity compared to the larger pile group configurations.

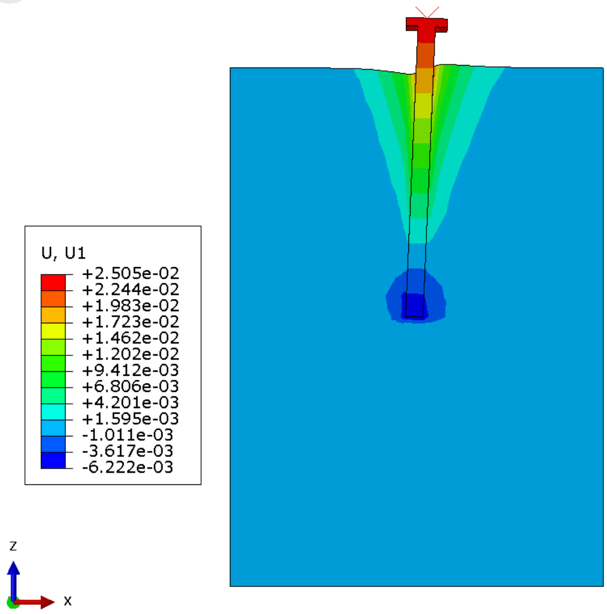

(a) CCFAT pile single

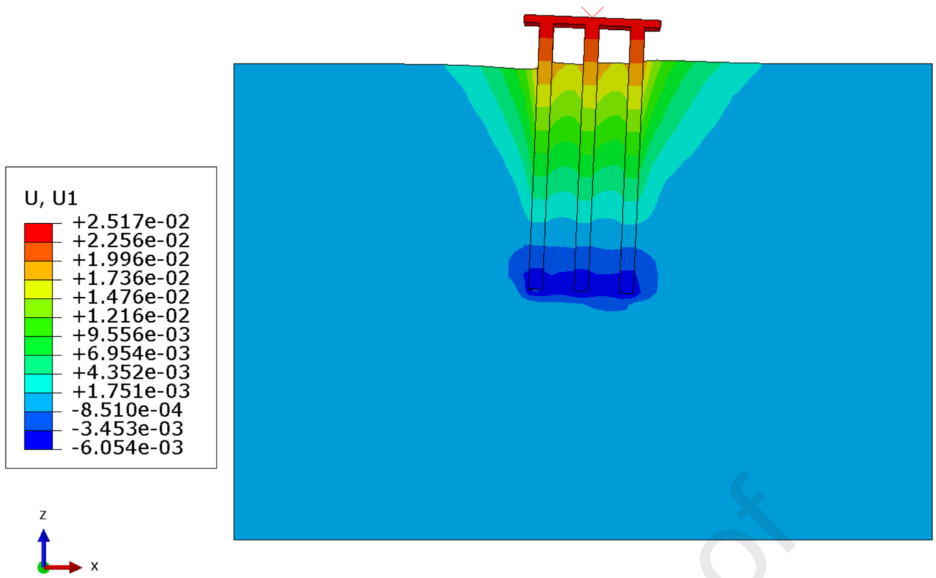

(b) 2x3 CCFAT pile group

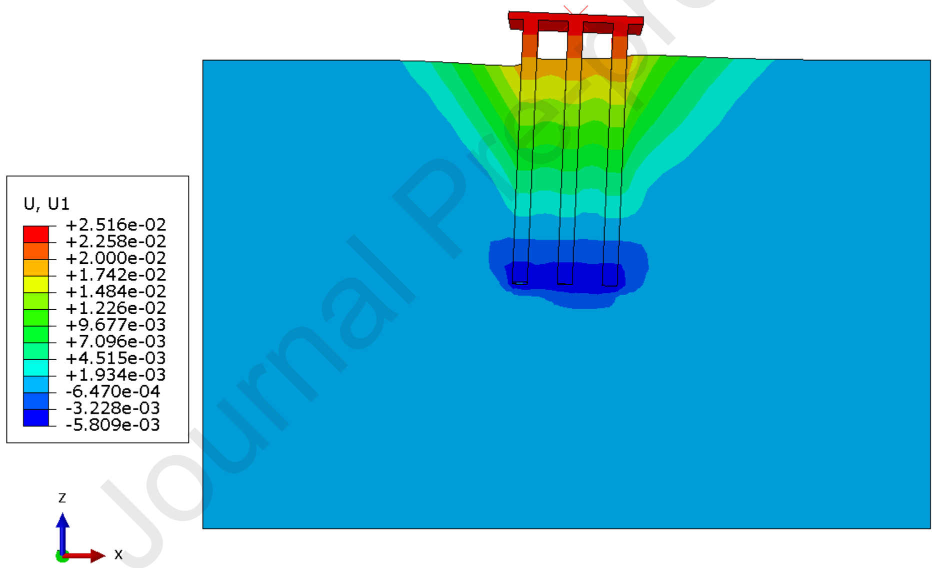

(c) 3x3 CCFAT pile group

Figure 17. Lateral displacement contours for CCFAT pile group under lateral loading

3.2.5. CCFAT pile sensitive analysis

Soil parameters, including the internal friction angle, dilatancy angle, Young's modulus, and friction coefficient between CCFAT piles and soil, play a pivotal role in the constitutive model, influencing bearing behavior [55, 63, 64]. While some parameters, such as the internal friction angle, can be measured through geotechnical tests, others, like the dilatancy angle, present measurement challenges, leading to imprecise determinations. Consequently, a meticulous investigation was conducted to assess the significance of these parameters in the Mohr-Coulomb soil model. Two control models, the 2x1 CCFAT pile group with L_m/D of 20 and the 2x2 CCFAT pile group with L_m/D of 10, were selected for vertical and lateral loading, respectively. For the parametric study, simulations were conducted using standard reference values for internal friction angle, dilatancy angle, Young's modulus, and friction coefficient, as listed in Table 9. It is worth mentioning the standard ultimate vertical and lateral load was presented for a loose sand model with a relative density (D_r) of 30%. These values were used as a baseline for the analysis. The parametric study was then performed by varying each parameter individually while keeping the others constant. Specifically, the internal friction angle was varied from 25° to 40°, the dilatancy angle from 2° to 10°, Young's modulus from 10 MPa to 40 MPa, and the friction coefficient from 0.2 to 0.5. This approach allowed for a comprehensive examination of the effects of each parameter on the behavior of pile group under vertical and lateral loading conditions [52, 65]. Additionally, care was taken to include sand density cases not covered in the experimental study, namely medium-dense and dense sand. To elucidate the impact of the aforementioned parameters, ultimate vertical capacity (P_{uv}) and ultimate lateral capacity (P_{ul}) were normalised against the standard ultimate vertical capacity of CCFAT pile group 2x1 with (L_m/D) 20 (P_{uvs}) and the standard ultimate lateral capacity of 2x2 with (L_m/D) 10 (P_{uls}), and the results were quantitatively represented in Figure 18 (a and b).

Table 9. Categorised soil parameters

Parameters	Values	Standard reference
Internal Friction Angle, Φ (°)	25, 35, 40	30
Dilatancy Angle, ψ (°)	2, 10, 15	5
Young's Modulus, E (MPa)	10, 30, 40	20
Friction Coefficient, K	0.2, 0.4, 0.5	0.3

The ultimate vertical capacities for the 2x1 CCFAT pile group with Lm/D of 20 are obtained as 550.7506, 1046.30, 1108.486 and 1653.965 for internal friction angles of 25°, 30°, 35° and 40°. For the same geometry, the ultimate vertical capacities are obtained as 1046.30, 559.73, 1379.47 and 2011.06 N, respectively, for the dilation angle values of 2°, 5°, 10°, 15°. As the Young's modulus values have been increased from 10, 20, 30 and 40 MPa, the ultimate vertical capacities are obtained as 647.98, 1046.30, 1265.57 and 1356.50 N, respectively. For the friction coefficient values of 0.2, 0.3, 0.4 and 0.5, respectively, the ultimate vertical capacities are obtained as 850.36, 1046.30, 1108.93 and 1185.17 N, respectively.

The influence of soil parameters on vertical loading is evident in Figure 18a. Both the internal friction angle and dilatancy angle emerged as key determinants of the vertical behavior of the CCFAT pile group. A linear relationship revealed a substantial increase in ultimate vertical capacity with an increasing dilatancy angle, reaching a variation of 140% within the dilatancy angle range of 2°–15°. Similarly, the effective internal friction angle exhibited a consistent upward trend, resulting in a total increase of 110%. Furthermore, an increase in Young's modulus contributed to the ultimate vertical load, but the growth decelerated gradually. With Young's modulus ranging from 10 MPa to 20 MPa, the ultimate vertical capacity increased by up to 38%. Conversely, when Young's modulus ranged from 30 MPa to 40 MPa, the increase in ultimate vertical capacity was less than 10%. The influence of Young's modulus was more pronounced in loose sand conditions (10–20 MPa) than in dense sand conditions (>30 MPa). In contrast, the friction coefficient between the pile and soil had a marginal effect, resulting in a 30% improvement within a reasonable range (0.2–0.5).

The ultimate lateral capacities for the 2x2 CCFAT pile group with L_m/D of 10 are obtained as 229.27, 467.9, 556.80 and 687.81 N for the angle of internal friction values of 25°, 30°, 35° and 40°, respectively. For the same geometry, as the dilatancy angle values are increased from 2°, 5°, 10° and

15^o, the ultimate lateral capacities are obtained as 299.46, 467.90, 519.37 and 575.52 N, respectively. The ultimate lateral capacities are obtained as 243.31, 467.90, 575.52 and 650.38 N, respectively, for the Young's modulus values of 10, 20, 30 and 40 MPa. For the friction coefficient values of 0.2, 0.3, 0.4 and 0.5, the ultimate lateral capacities are obtained as 397.71, 467.90, 500.65 and 547.44 N, respectively.

Considering lateral loading, as depicted in Figure 18b, internal friction and Young's modulus emerged as significant factors influencing the lateral behavior of the CCFAT pile group. The ultimate lateral capacity exhibited a substantial increase with an increasing internal friction angle, reaching an 82% variation within the internal friction angle range of 25^o–40^o. The effective Young's modulus showed a similar pattern, with a 79% increase. However, this demonstrated that the influence of Young's modulus was less effective in dense sand conditions. Additionally, the ultimate lateral capacity increased with an increasing dilatancy angle, showing a unique trend, and resulting in a total increase of 45%. The friction coefficient between the pile and soil had a slight effect, leading to a 25% improvement within a reasonable range of friction coefficients (0.2–0.5).

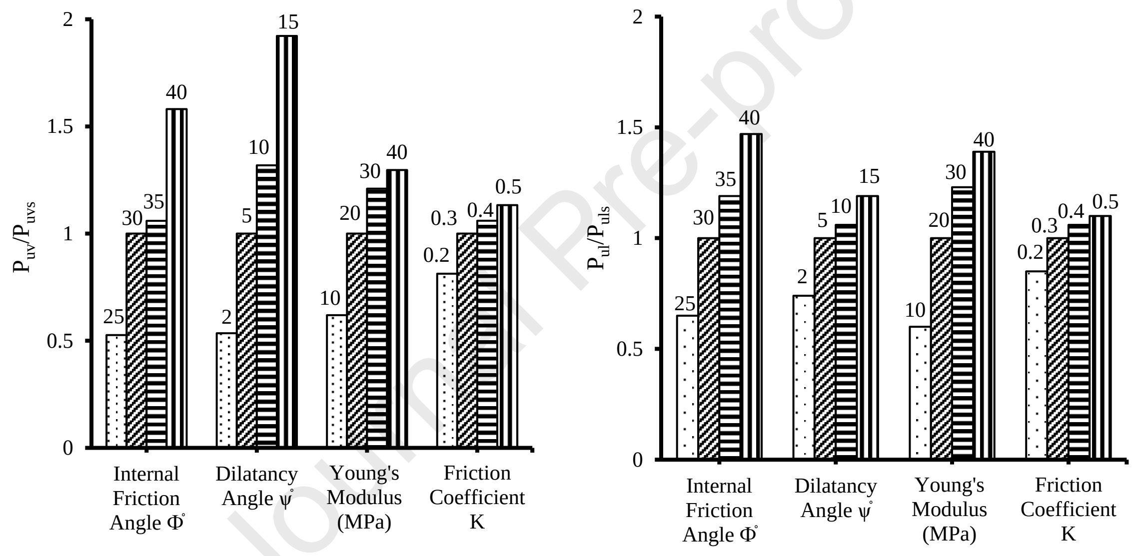

(a) Vertical loading (b) Lateral loading

Figure 18. Sensitive analysis of soil parameters to CCFAT pile

4. Conclusion

The main aim of this research was to comprehensively investigate the performance of composite piles, both in singular form and when organised into pile groups, under the influence of vertical and lateral loading. Both experimental works via scaled models and finite element (FE) simulations using ABAQUS software were conducted in this research. As part of the experimental work, comparative analyses were conducted to compare the performance of the Confined Concrete-Filled Aluminum Tube (CCFAT) pile models against Hollow Aluminum Tube (HAT), and Precast Concrete (PC) piles under vertical and lateral loading capacity. According to the obtained results, the following conclusions were drawn:

1- The P_{uv} of the CCFAT pile model were close to that of the PC pile model and twice that of the HAT pile model under constant L_m/D ratio, load conditions and soil properties. Additionally, it was found that the P_{ul} of the CCFAT pile model was 1.5 and 2.5 times that of the PC and HAT models, respectively.
2- Both ultimate vertical and later capacity increase with the increase of L_m/D.

3- The relationship between the vertical load and vertical settlement curves follows a linear and pronounced slope trend, while the relationship between the lateral load and lateral displacement curves follows a nonlinear, rapidly changed slope.
4- Due to the pile stiffness of the CCFAT pile, the maximum bending moment depth remains constant for the L_m/D 10 model and marginally increases in the L_m/D 20 under the lateral loads. However, the down-row pile consistently exhibits, at the same lateral displacement, a greater resistance to bendin moment than its up-row counterpart in the CCFAT pile group 2x2.
5- The FE simulations highly agreed with the experimental results for various CCFAT pile models at different L_m/D ratios and configurations under both vertical and lateral loads.
6- Both ultimate vertical and lateral capacities were increased with the increase of pile number. However, detectable differences in the increase rates compared to the single piles.
7- The developed fitted charts could be used as a tool for estimating the ultimate vertical and lateral capacities of CCFAT pile groups based on pile group stiffness.
8- Using two and three rows of the CCFAT pile group under lateral loading results in the upward movement of the soil along the up-row piles and the generation of tension force. Conversely, a downward movement of the soil took place along the down-row piles, and it generated a compression force. Notably, the soil movement in front of the middle pile was relatively negligible.
9- The sensitivity analysis indicated that both the dilatancy angle and internal friction angle exert a considerable influence on the ultimate vertical capacity of the CCFAT pile group. Additionally, it was noticed that the internal friction angle and Young's modulus are pivotal factors affecting the ultimate lateral capacity of the CCFAT pile group. The impact of Young's modulus was more pronounced in loose sand.

In conclusion, this study introduces an effective approach for estimating the ultimate vertical and lateral capacity of a novel composite (CCFAT) pile. It is important to note that the configuration utilized is representative of common pile group layouts. However, there is a need for further investigations to validate and refine this method for unique and specialized configurations. Future research should also explore the influence of combined loading conditions (vertical and lateral), particularly in marine environments, on the performance of CCFAT piles. Ultimately, these findings may prove instrumental in the development of design charts and equations, offering optimal guidance for the utilization of composite piles by researchers and engineers.

The symbols utilized in this study are as follows:

C_c = Coefficient of curvature
C_u = Coefficient of uniformity
D = pile diameter
D_{50} =medium diameter of the sand
D_{10} = Sand Effective size
D_{30} = Effective size
D_r = Relative density
E = Young's modulus of soil
E_a= Young's modulus of aluminium
E_c= Young's modulus of concrete infill
fc = Concrete cubes compressive strength

G_s = Specific gravity
I_a = Moment of inertia of aluminium
I_c = Moment of inertia of concrete infill
K = Friction coefficient
K_e = correction factor for concrete
L_m/D = Slenderness ratios
P_l = Lateral load
P_{ul} = Ultimate lateral load
P_{ulg} = Ultimate lateral capacity of the pile group
P_{uls} = Ultimate lateral capacity of single pile
P_{uv} = Ultimate vertical load
P_{uvg} = Ultimate vertical capacity of the pile group
P_{uvs} = Ultimate vertical capacity of single pile
P_v = Vertical load
S = Centre to-centre distance between piles
Φ° = Internal Friction Angle
ψ° =Dilatancy Angle
η_l = Pile group stiffness factor under lateral load
η_v = Pile group stiffness factor under vertical load
γ = Sand desnsity
γ_{max} = Maximum sand desnsity
γ_{min} = Minimum sand desnsity
γ_d = Dray sand density

Conflict of interest

The authors declare that no conflict of interest.

References

1. Hosseini, M.A. and M.T. Rayhani, *Seismic response of end-bearing fibre-reinforced polymer (FRP) piles in cohesionless soils.* Innovative Infrastructure Solutions, 2021. **7**(1): p. 56-69.
2. Ateş, B. and E. Şadoğlu, *Experimental and Numerical Investigation of Load Sharing Ratio for Piled Raft Foundation in Granular Soils.* KSCE journal of civil engineering., 2022. **26**(4): p. 1662-1673.
3. Firoj, M. and B.K. Maheshwari, *Effect of CPRF on nonlinear seismic response of an NPP structure considering raft-pile-soil-structure-interaction.* Soil dynamics and earthquake engineering, 2022. **158**: p. 107295.
4. Ateş, B. and E. Şadoğlu, *Experimental investigation of pile addition and length on bearing capacity and settlement of rafts on loose sandy soil.* Afyon Kocatepe Üniversitesi Fen Ve Mühendislik Bilimleri Dergisi, 2021. **21**(2): p. 399-407.
5. Limkatanyu, S., et al., *Improved nonlinear displacement-based beam element on a two-parameter foundation.* European journal of environmental and civil engineering., 2015. **19**(6): p. 649-671.
6. Al-Darraji, F., et al., *A Systematic Review of the Geotechnical and Structural Behaviors of Fiber-Reinforced Polymer Composite Piles.* Geosciences, 2023. **13**(3): p. 78.
7. Zyka, K. and A. Mohajerani, *Composite piles: A review.* Construction & building materials, 2016. **107**: p. 394-410.
8. Mirmiran, A., Y. Shao, and M. Shahawy, *Analysis and field tests on the performance of composite tubes under pile driving impact.* Composite Structures, 2002. **55**(2): p. 127-135.

9. Fam, A., et al., *Precast piles for Route 40 bridge in Virginia using concrete filled FRP tubes.* PCI journal, 2003. **48**(3): p. 32-45.
10. Giraldo, J. and M.T. Rayhani, *Load transfer of hollow Fiber-Reinforced Polymer (FRP) piles in soft clay.* Transportation Geotechnics, 2014. **1**(2): p. 63-73.
11. Giraldo Valez, J. and M.T. Rayhani, *Axial and lateral load transfer of fibre-reinforced polymer (FRP) piles in soft clay.* International journal of geotechnical engineering, 2017. **11**(2): p. 149-155.
12. Lu, Y., et al., *Preliminary Study on the Behaviour of Fibre-Reinforced Polymer Piles in Sandy Soils.* Buildings, 2022. **12**(8): p. 1-17.
13. Almallah, A., H. El Naggar, and P. Sadeghian, *Axial Behavior of Innovative Sand-Coated GFRP Piles in Cohesionless Soil.* International Journal of Geomechanics, 2020. **20**(10): p. 04020179.
14. Venkatesan, G., et al., *Experimental investigation on load carrying capacity of hollow and composite pile materials in layered soil.* Materials Today: Proceedings, 2022. **65**(9): p. 3951-3958.
15. Ilyas, T., et al., *Centrifuge Model Study of Laterally Loaded Pile Groups in Clay.* Journal of geotechnical and geoenvironmental engineering, 2004. **130**(3): p. 274-283.
16. Wen, K., X. Wu, and B. Zhu, *Numerical investigation on the lateral loading behaviour of tetrapod piled jacket foundations in medium dense sand.* Applied ocean research, 2020. **100**: p. 102193.
17. Majumder, M., D. Chakraborty, and V. Kumawat, *Model test study on single and group under-reamed piles in sand under compression and tension.* Innovative Infrastructure Solutions, 2022. **7**(1): p. 129.
18. Wang, Z., et al., *Numerical investigation of the lateral response of pile groups in sand under local scour conditions.* Computers and Geotechnics, 2023. **159**: p. 105435.
19. Abu-Farsakh, M., A. Souri, and G. Voyiadjis, *Numerical Simulation of a Barge Impact on Bridges with Different Configurations of Pile Group Foundations.* Transportation Research Record, 2023. **2677**(12): p. 128-143.
20. Wang, X., S. Li, and J. Li, *Experimental and numerical study on lateral response of pile-group for offshore wind turbines in sand.* Marine Georesources & Geotechnology, 2023. **41**(5): p. 524-543.
21. Limkatanyu, S., et al., *Nonlinear shear-flexure-interaction RC frame element on Winkler-Pasternak foundation.* Geomechanics and Engineering, 2023. **32**(1): p. 69-84.
22. Pujiastuti, H., et al., *Single piles and pile groups capacity in unsaturated sandy clay based on laboratory test.* ASEAN Engineering Journal, 2022. **12**(1): p. 165-171.
23. Georgantzia, E., et al., *Flexural buckling performance of concrete-filled aluminium alloy tubular columns.* Engineering Structures, 2021. **242**: p. 112546.
24. Comodromos, E.M., M.C. Papadopoulou, and I.K. Rentzeperis, *Pile foundation analysis and design using experimental data and 3-D numerical analysis.* Computers and geotechnics, 2009. **36**(5): p. 819-836.
25. Ates, B. and E. ŞAdoĞLu, *Experimental investigation of optimum piles spacing for piled raft foundation in sandy soils.* Teknik Dergi, 2021. **32**(1): p. 10477-10493.
26. Rathod, D., K. Muthukkumaran, and S.G. Thallak, *Experimental Investigation on Behavior of a Laterally Loaded Single Pile Located on Sloping Ground.* International journal of geomechanics., 2019. **19**(5): p. 04019021.
27. British Standards Institute, *BS 1377-2:2022: Methods of test for soils for civil engineering purposes: Classification tests and determination of geotechnical properties*. 2022, British Standards Institute.
28. Jebur, A.A., et al., *Artificial neural network (ANN) approach for modelling of pile settlement of open-ended steel piles subjected to compression load.* European Journal of Environmental and Civil Engineering, 2021. **25**(3): p. 429-451.

29. Garnier, J., et al., *Catalogue of scaling laws and similitude questions in geotechnical centrifuge modelling.* International Journal of Physical Modelling in Geotechnics, 2007. **7**(3): p. 01-23.
30. Basack, S., *A Technical Note on Development and Performance Study of a Set-up for Imparting Lateral Cyclic Load on Piles.* Marine Georesources & Geotechnology, 2009. **27**(4): p. 322-341.
31. Khari, M., K.A. Kassim, and A. Adnan, *An Experimental Study on Pile Spacing Effects under Lateral Loading in Sand.* TheScientificWorld, 2013. **2013**: p. 734292-8.
32. Madhusudan Reddy, K. and R. Ayothiraman, *Experimental studies on behavior of single pile under combined uplift and lateral loading.* Journal of geotechnical and geoenvironmental engineering, 2015. **141**(7): p. 04015030.
33. Al-abboodi, I. and T.T. Sabbagh, *Model tests on piled raft subjected to lateral soil movement.* International Journal of Geotechnical Engineering, 2018. **12**(4): p. 357-367.
34. Ateş, B. and E. Şadoğlu, *Experimental investigation for group efficiency of driven piles embedded in cohesionless soil.* KSCE Journal of Civil Engineering, 2023. **27**(12): p. 5123-5134.
35. Ateş, B. and E. Şadoglu, *Experimental and numerical investigation for vertical stress increments of model piled raft foundation in sandy soil.* Iranian Journal of Science and Technology, Transactions of Civil Engineering, 2022. **46**(1): p. 309-326.
36. Rollins, K.M., K.T. Peterson, and T.J. Weaver, *Lateral load behavior of full-scale pile group in clay.* Journal of geotechnical and geoenvironmental engineering, 1998. **124**(6): p. 468-478.
37. Han, J., J.D. Frost, and V.L. Brown, *Design of fiber-reinforced polymer composite piles under vertical and lateral loads.* Transportation research record, 2003. **1849**(1): p. 71-80.
38. Thangavel, J.K., D. Rathod, and S. Govindaraj, *Behavior of a Laterally Loaded Rigid Finned Pile Located on a Sloping Ground Surface.* International journal of geomechanics., 2024. **24**(4): p. 04024045.
39. Nigitha, D., D. Rathod, and K.T. Krishnanunni, *Finite-element analysis of a monopile under one- and two-way lateral cyclic loading.* Proceedings of the Institution of Civil Engineers., 2023. **176**(3): p. 138-157.
40. Qu, L., et al., *Vertical dynamic interaction and group efficiency factor for floating pile group in layered soil.* International Journal for Numerical and Analytical Methods in Geomechanics, 2023. **47**: p. 1953-1978.
41. McCabe, B.A. and B.M. Lehane, *Behavior of Axially Loaded Pile Groups Driven in Clayey Silt.* Journal of geotechnical and geoenvironmental engineering., 2006. **132**(3): p. 401-410.
42. Das, B.M. and N. Sivakugan, *Principles of foundation engineering*. 2018: Cengage learning.
43. Krishnanunni, K.T. and D. Rathod, *Behaviour of a laterally loaded short-finned pile located on sloping ground.* International journal of physical modelling in geotechnics., 2024. **24**(3): p. 110-123.
44. Li, Z., et al., *Capacity Change of Piles in Loess under Cyclic Axial Tension or Compression Load.* International Journal of Geomechanics, 2023. **23**(10): p. 04023182.
45. Gao, Z. and J. Zhao, *Strain localization and fabric evolution in sand.* International Journal of Solids and Structures, 2013. **50**(22-23): p. 3634-3648.
46. Timoshenko, S., *Elementary theory and problems*. 1940: Van Nostrand.
47. Patel, V.I., Q.Q. Liang, and M.N.S. Hadi, *Numerical simulations of circular high strength concrete-filled aluminum tubular short columns incorporating new concrete confinement model.* Thin-Walled Structures, 2020. **147**: p. 106492.
48. Azad, S.K., D. Li, and B. Uy, *Compact and slender box concrete-filled stainless steel tubes under compression, bending, and combined loading.* Journal of Constructional Steel Research, 2021. **184**: p. 106813.
49. McAdam, R.A., et al., *Monotonic laterally loaded pile testing in a dense marine sand at Dunkirk.* Géotechnique, 2020. **70**(11): p. 986-998.

50. T, J.K., D. Rathod, and S.K. Sahoo, *Behaviour of a laterally loaded rigid helical pile located on a sloping ground surface.* Marine georesources & geotechnology., 2024: p. 1-20.
51. Deendayal, R., K. Muthukkumaran, and T.G. Sitharam, *Analysis of laterally loaded group of piles located on sloping ground.* International journal of geotechnical engineering., 2020. **14**(5): p. 580-588.
52. Wang, X., S. Li, and J. Li, *Effect of pile arrangement on lateral response of group-pile foundation for offshore wind turbines in sand.* Applied Ocean Research, 2022. **124**: p. 103194.
53. Manual, A.S.U.s., *Abaqus 6.11.* http://130.149, 2012. **89**(2080): p. v6.
54. Wang, J., et al., *Finite element analyses of improved lateral performance of monopile when combined with bucket foundation for offshore wind turbines.* Applied Ocean Research, 2021. **111**: p. 102647.
55. Deb, T.K. and B. Singh, *Response and capacity of monopod caisson foundation under eccentric lateral loads.* Marine Georesources & Geotechnology, 2018. **36**(4): p. 452-464.
56. Sae-Long, W., et al., *Nonlinear winkler-based frame element with inclusion of shear-flexure interaction effect for analysis of non-ductile RC members on foundation.* Journal of Applied and Computational Mechanics, 2021. **7**(1): p. 148-164.
57. Al-abboodi, I. and T.T. Sabbagh, *Numerical modelling of passively loaded pile groups.* Geotechnical and Geological Engineering, 2019. **37**(4): p. 2747-2761.
58. Limkatanyu, S., et al., *Shear-flexure Interaction Frame Model on Kerr-type Foundation for Analysis of Non-ductile RC Members on Foundation.* Journal of Applied and Computational Mechanics, 2022. **8**(3): p. 1076-1090.
59. Bhowmik, D., D.K. Baidya, and S.P. Dasgupta, *A numerical and experimental study of hollow steel pile in layered soil subjected to vertical dynamic loading.* Soil dynamics and earthquake engineering, 2016. **85**: p. 161-165.
60. Sayed, S.M. and R.M. Bakeer, *Efficiency formula for pile groups.* Journal of geotechnical engineering, 1992. **118**(2): p. 278-299.
61. Vakili, A., S.M.A. Zomorodian, and H. Bahmyari, *Group Reduction Factors for the Analysis of the Pile Groups Under Combination of Lateral Loads in Sandy Soils.* Transportation Infrastructure Geotechnology, 2023. **10**: p. 1-21.
62. Cao, M. and A. Zhou, *Fictitious pile method for fixed-head pile groups with dissimilar piles subjected to horizontal loading.* Soils and Foundations, 2022. **62**(5): p. 101212.
63. Yang, X., X. Zeng, and X. Wang, *Lateral-moment loading capacity and bearing behavior of suction bucket foundations for offshore wind turbines in sand.* International Journal of Geomechanics, 2018. **18**(11): p. 04018152.
64. Achmus, M., C.T. Akdag, and K. Thieken, *Load-bearing behavior of suction bucket foundations in sand.* Applied Ocean Research, 2013. **43**: p. 157-165.
65. Faizi, K., *Numerical and Experimental Investigation of Novel Foundation Systems for Offshore Wind Turbines*. 2020, University of Birmingham.

The composite piles are the alternative to traditional piles.

The Innovative CCFAT pile added the structural advantages of aluminium and concrete.

The rigidity of CCFAT piles played a role in the bending moment.

New charts to estimate the ultimate vertical and lateral capacities are proposed.

Soil properties have disparately influenced the behavior of the CCFAT pile.

Declaration of interests

The authors declare that they have no known competing financial interests or personal relationships that could have appeared to influence the work reported in this paper.

Fadhil Al-Darraji
26/07/2024